Biogeosciences, 7, 1789–1807, 2010
www.biogeosciences.net/7/1789/2010/
doi:10.5194/bg-7-1789-2010

Biogeosciences

Trends of anthropogenic CO_2 storage in North Atlantic water masses

F. F. Pérez[1], **M. Vázquez-Rodríguez**[1], **H. Mercier**[2], **A. Velo**[1], **P. Lherminier**[2], **and A. F. Ríos**[1]

[1]Instituto de Investigaciones Marinas, CSIC, Eduardo Cabello 6, 36208 Vigo, Spain
[2]Laboratoire de Physique des Océans, CNRS Ifremer IRD UBO, IFREMER Centre de Brest, B.P. 70 29280 Plouzané, France

Received: 29 November 2009 – Published in Biogeosciences Discuss.: 13 January 2010
Revised: 26 April 2010 – Accepted: 30 April 2010 – Published: 28 May 2010

Abstract. A high-quality inorganic carbon system database, spanning over three decades (1981–2006) and comprising of 13 cruises, has allowed the applying of the φC_T° method and coming up with estimates of the anthropogenic CO_2 (C_{ant}) stored in the main water masses of the North Atlantic. In the studied region, strong convective processes convey surface properties, like C_{ant}, into deeper ocean layers and grants this region an added oceanographic interest from the point of view of air-sea CO_2 exchanges. Generally, a tendency for decreasing C_{ant} storage rates towards the deep layers has been observed. In the Iberian Basin, the North Atlantic Deep Water has low C_{ant} concentrations and negligible storage rates, while the North Atlantic Central Water in the upper layers shows the largest C_{ant} values and the largest annual increase of its average concentration ($1.13 \pm 0.14\,\mu mol\,kg^{-1}\,yr^{-1}$). This unmatched rate of change in the C_{ant} concentration of the warm upper limb of the Meridional Overturning Circulation decreases towards the Irminger basin ($0.68 \pm 0.06\,\mu mol\,kg^{-1}\,yr^{-1}$) due to the lowering of the buffering capacity. The mid and deep waters in the Irminger Sea show rather similar C_{ant} concentration rates of increase (between 0.33 and $0.45\,\mu mol\,kg^{-1}\,yr^{-1}$), whereas in the Iceland basin these layers seem to have been less affected by C_{ant}. Overall, the C_{ant} storage rates in the North Atlantic subpolar gyre during the first half of the 1990s, when a high North Atlantic Oscillation (NAO) phase was dominant, are ∼48% higher than during the 1997–2006 low NAO phase that followed. This result suggests that a net decrease in the strength of the North Atlantic sink of atmospheric CO_2 has taken place during the present decade. The changes in deep-water ventilation are the main driving processes causing this weakening of the North Atlantic CO_2 sink.

Correspondence to: F. F. Pérez
(fiz.perez@iim.csic.es)

1 Introduction

The North Atlantic is known as the most important anthropogenic CO_2 (C_{ant}) sink of the global ocean (Sabine et al., 2004). Recent studies and future scenarios from the International Panel on Climate Change (IPCC, 2007) point towards a decline in the intensity of the Meridional Overturning Circulation (MOC) in the next 100 years. The observed weakening of the North Atlantic subpolar gyre (NASPG) during the 1990s seems to have been driven by the North Atlantic Oscillation (NAO), i.e., caused by the changes in wind stress and heat flux as part of the decadal variability of the gyre transport (Häkkinen and Rhines, 2004). Notably, such changes in the subpolar gyre reverberate in the strength of the MOC in the subtropical North Atlantic (Böning et al., 2006). The Hurrell NAO winter index is computed as the difference of surface atmospheric pressure between Iceland and Azores (timeseries values available at www.cgd.ucar.edu/cas/jhurrell/indices.html). On the other hand, the greenhouse-enhanced temperature rise and freshwater fluxes in the high latitudes, where water mass formation processes abound, can potentially contribute to the weakening of MOC intensity. Although the effects of the MOC slowdown are still a matter of debate (Swingedouw et al., 2007), it is likely that they will cast profound consequences on global climate due to the associated decrease in heat transport (Drijfhout et al., 2006) and oceanic C_{ant} uptake (Sarmiento and Le Quéré, 1996).

The Labrador Sea Water (LSW) is one of the thickest water masses in the North Atlantic, and one of the main components of the lower limb of MOC that flows southwards. Several Ocean General Circulation Models (OGCMs) have suggested that the decadal variability of the MOC is closely related with the variability of LSW formation rates (Böning et al., 2006; Latif et al., 2006; Steinfeldt et al., 2009).

Published by Copernicus Publications on behalf of the European Geosciences Union.

The water column stratification and wind forcing intensity are determining factors in the efficiency of convective processes (Dickson et al., 1996; Curry et al., 1998; Lazier et al., 2002). Convection activity in the Labrador Sea is related to the persistence and phase of the NAO. In the early 90s (1989–1995) the 5-year mean ± standard deviation of this index was 3.3 ± 0.8 indicating a high phase of the NAO. A low NAO phase period followed during the years 1996–2006, when the index value dropped to -0.1 ± 0.6. A positive NAO phase causes stronger winds and heat loss in the Labrador Sea, fostering convection. During the early 1990s, the highly positive phase of the NAO coincided with an impressive and exceptional convection activity down to more than 2000 m (Dickson et al., 1996; Lazier et al., 2002; Yashayaev et al., 2008). The enhanced convection provoked the formation of the thickest layer of classical LSW (*c*LSW) observed in the past 60 years (Curry et al., 1998). However, this high LSW formation period that started in 1988 (Sy et al., 1997) ended abruptly in 1996 with the shift from high to a low NAO phase. Nonetheless, weaker convection events (to less than 1000 m in depth, on average) continued to take place in the central Labrador Sea region and formed the less dense upper LSW (*u*LSW).

The present work examines the temporal variability of C_{ant} storage in the main water masses of the North Atlantic (>40° N). This region is a fast-track entrance portal for C_{ant} to the deep ocean through the overturning circulation driven by deep convection (Kieke et al., 2007; Pérez et al., 2008). By applying the $\varphi\, C_T^\circ$ C_{ant} estimation method (Pérez et al., 2008; Vázquez-Rodríguez et al., 2009a), we aim to study and quantify the changes in C_{ant} storage rates that occurred in the North Atlantic since the early 1980s. The changes can be provoked by the actual changes in the amounts of C_{ant} that are being stored in the ocean (as a direct consequence of rising atmospheric CO_2 levels) and by the changes in the volumetric census of the main water masses involved in this region (Steinfeldt et al., 2009). These two processes will be evaluated in this work.

2 Dataset

A total of thirteen cruises with high-quality carbon system measurements were selected to study the temporal evolution of C_{ant} in the North Atlantic. The combined dataset spans over 25 years (1981–2006) and gives a comprehensive spatial coverage of the area (Fig. 1a; Table 1), with an emphasis on important water mass transformation areas like the Irminger and Iceland basins. The geographical boundaries of the Irminger basin have been established between the main axis of the Reykjanes Ridge and the east coast of Greenland (Fig. 1a). Likewise, the Iceland basin is defined as the region enclosed between the Reykjanes Ridge axis and the line joining the Eriador Seamount and the Faroe Islands. The region designated as Eastern North Atlantic basin (ENA basin

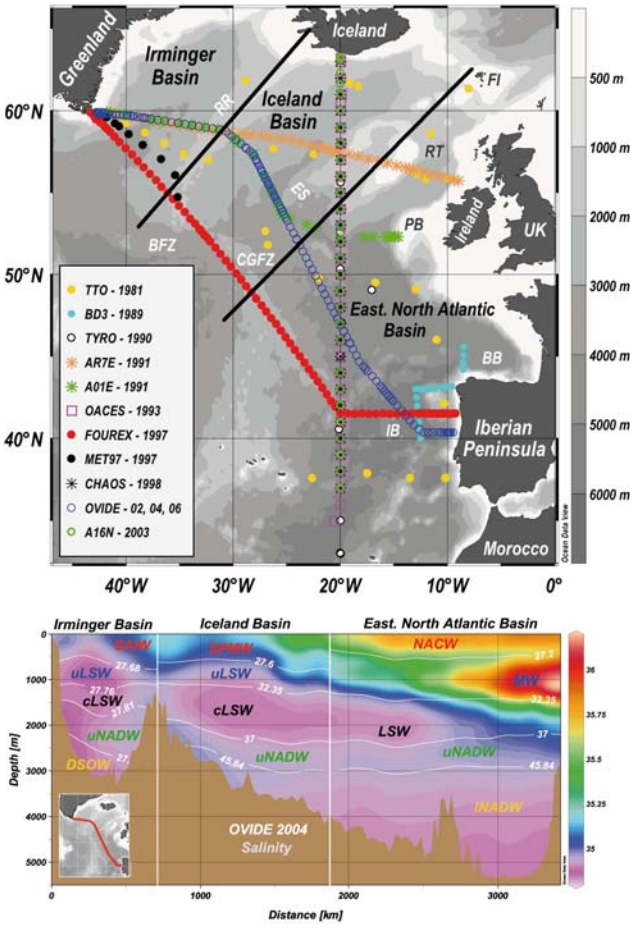

Fig. 1. Fig. 1a shows the tracks of the thirteen cruises used in this study, spanning twenty-seven years of marine carbon system measurements. The greyscale on the sidebar indicates depth (m). The two black straight lines are the boundaries selected to distinguish and designate the Irminger, Iceland and ENA basins. Some of the TYRO stations are inevitably masked under the CHAOS, OACES and A16N cruise symbol sets. Acronyms for the underwater and coastal topography denote the following: RR= Reykjanes Ridge; BFZ= Bight Fracture Zone; CGFZ= Charlie-Gibbs Fracture Zone; ES= Eriador Seamount; FI= Faroe Islands; RT= Rockall Trough; PB= Porcupine Bank; BB= Biscay Basin; IB=Iberian Basin. Figure 1b displays the observed salinity field for the OVIDE '04 section, which representatively covers the latitudinal and longitudinal ranges of the studied region. The selected boundary isopycnals (potential density "σ", in kg m^{-3}) used to demarcate and follow the C_{ant} evolution of the main water masses in the Irminger, Iceland and ENA basins are also shown. Surface is generally taken as the reference pressure level for the isopycnals (σ_0, ref. press. = 0 dbar), except for the intermediate and deep waters on the Iceland and ENA basins, where 1000, 2000 and 4000 dbar are the references for the σ_1=32.35; σ_2=37.00 and σ_4=45.84 kg m^{-3} isopycnals, respectively. Water mass acronyms mean the following: SAIW= Sub Arctic Intermediate Water; LSW = Labrador Sea Water; NADW = North Atlantic Deep Water; SPMW = Sub Polar Mode Water; NACW = North Atlantic Central Water; MW = Mediterranean Water. The lowercase first letters "*c*", "*u*" and "*l*" denote the "classical", "upper" and "lower" varieties in some water masses, respectively.

Table 1. North Atlantic cruises (Fig. 1). P.I.=Principal Investigator; n.a.=no adjustment made. The EXPOCODE is the "expedition code", a unique alphanumeric identifier that generally has the format "*NODCYYYYMMDD*", where *NODC* is NOAA's National Oceanographic Data Center's 4-character research vessel identifier (http://www.nodc.noaa.gov/General/NODC-Archive/platformlist.txt) and *YYYYMMDD* is the GMT date when the cruise left port. The FOUREX, CHAOS and OVIDE cruises reported to the CARINA database spectrophotometric pH measurements (Clayton and Byrne, 1993) in the total scale (pH_T), while the BD3 did it in SWS scale (pH_{SWS}). The adjustments from pertinent a posteriori crossover analysis (Pierrot et al., 2010; Velo et al., 2009a, b) are given in µmol kg^{-1} for C_T and A_T and in pH units for pH.

Cruise Information						Adjustments		
Section	Year	P.I.	EXPOCODE	Number of Stations	Number of Samples	pH	C_T	A_T
TTO	1981	T. Takahashi	316N19810923	30	591	n.a.	−3.0	−3.6
BD3	1989	M. Arhan	35LU19890509	20	218	0.024	n.a.	n.a.
TYRO	1990	G. Fransz	64TR19900417	11	189	n.a.	n.a.	14
AR7E	1991	H. M. van Aken	64TR19910408	30	616	n.a.	6	n.a.
A01E	1991	J. Meincke	06MT18-1	26	431	n.a.	n.a.	n.a.
OACES	1993	R. Wanninkhof	OACES93	28	497	n.a.	n.a.	n.a.
FOUREX	1997	S. Bacon	74DI19970807	83	1458	−0.005	n.a.	n.a.
MET97	1997	F. Schott	06MT19970707	8	148	n.a.	n.a.	n.a.
CHAOS	1998	Smythe – Wright	74DI19980423	26	459	0.018	n.a.	−8.5
OVIDE '02	2002	H. Mercier	35TH20020611	85	1829	n.a.	n.a.	n.a.
A16N	2003	J. Bullister – N. Gruber	33RO20030604	25	693	n.a.	n.a.	n.a.
OVIDE '04	2004	T. Huck	35TH20040604	98	2091	n.a.	n.a.	n.a.
OVIDE '06	2006	P. Lherminier	06M220060523	89	1937	n.a.	n.a.	n.a.

hereinafter) extends south from the Eriador-Faroe line over the Rockall trough, the Porcupine bank, and the Biscay and Iberian basins.

Only bottle data that included carbon system analysis were used in this study. Some of the older cruises considered here did not use certified reference materials (CRMs) for their carbon system measurements, given the year they were conducted in. Also, the determination procedures varied between cruises, especially before OACES in 1993. These differences in the analytics have an effect on the precision attainable for a given carbon variable. In any case, the high quality of carbon measurements was one of the main criteria considered for cruise selection, i.e., all data are compliant with the latest carbon system analytical recommendations for seawater (DOE, 1994). They were accessed from the Carbon In the Atlantic (CARINA) data portal (http://store.pangaea.de/Projects/CARBOOCEAN/carina/index.htm), except for the OVIDE '06 data.

The annual averages from the World Ocean Atlas 2005 climatology (WOA05; http://www.nodc.noaa.gov/OC5/WOA05/woa05data.html) have been additionally used as references for normalizing layer thicknesses and tracer concentrations to basin-wide averages, given the heterogeneous and eventually sparse spatial coverage in some areas (Fig. 1a). This has occurred in spite of having used a comprehensive amount of thirteen cruises that met the desired data quality and give good temporal coverage at the same time. The WOA05 database provides annual, seasonal and monthly averages of several tracers for grid resolutions of $1^\circ \times 1^\circ$ and $5^\circ \times 5^\circ$ over 33 depth levels. In this study, we have used the annual average data with a $1^\circ \times 1^\circ$ grid resolution.

The pH was determined either potentiometrically (Dickson, 1993a, b) using pH electrodes or, more commonly, with a spectrophotometric method (Clayton and Byrne, 1993) adding *m*-cresol purple as an indicator in either scanning or diode array spectrophotometers. The spectrophotometric pH determination has typical precision limits of 0.002 pH units (Clayton and Byrne, 1993; Millero, 2007). Occasionally, the pH measurement protocols of the FOUREX and OVIDE cruises included periodical CRM checks that allowed for achieving a precision of 0.0014. The spectrophotometric measurements of pH of the FOUREX, CHAOS and all three OVIDE cruises were reported to the CARINA database in total scale (pH_T) and the BD3 in the SWS scale (pH_{SWS}). In any case, pH measurements were only used in this work to calculate either total inorganic carbon (C_T) from total alkalinity (A_T) and pH or A_T from C_T and pH, following the recommendations and guidelines from Velo et al. (2009b). The C_T and A_T variables are necessary to calculate C_{ant} with the φC_T° method (Pérez et al., 2008; Vázquez-Rodríguez et al., 2009a), while pH is not an input parameter in the φC_T° equations. The thermodynamic equations of the carbon system and the CO_2 dissociation constants from Dickson and Millero (1987) were used in all cases to make such A_T and C_T calculations.

All shipboard A_T samples were analysed with potentiometric titration and determined by developing either a full titration curve (Millero et al., 1993; DOE, 1994; Ono et al., 1998) or from single point titration (Pérez and Fraga, 1987; Mintrop et al., 2002). The C_T samples were analysed with Single Operator Multiparameter Metabolic Analyzers (SOMMA apparatus) based on coulometric titration techniques (Johnson et al., 1993) and were calibrated with CRMs. The exception to the latter is the 1981 TTO cruise, where C_T was determined potentiometrically (Bradshaw et al., 1981) and no CRMs were used. Also with respect to this cruise, Tanhua and Wallace (2005) performed a cross-over analysis between the TTO and an overlapping more recent cruise. Based on a comparison with CRM-referenced data, they suggested a correction for TTO-NAS C_T measurements of $-3.0\,\mu mol\,kg^{-1}$, which has been applied to our dataset. The analytical accuracies for C_T, A_T and pH were equal to or better than $\pm 2\,\mu mol\,kg^{-1}$, $\pm 4\,\mu mol\,kg^{-1}$ and ± 0.003 pH units, respectively. As specified in Table 1, an analysis exercise performed by the CARBOOCEAN Atlantic Synthesis group examined all existing Atlantic cruise crossovers and, for a few cruises, suggested corrections to the carbon system dataset (Pierrot et al., 2010; Velo et al., 2009a; Velo et al., 2009b).

The AR07E and A01E cruises deserved special treatment: The geographic position and timely date of these two cruises made them assets to this study. Both cruises had comprehensive amounts of coulometric C_T measurements yet very few potentiometric A_T data. Given the shortage of A_T data, they were not discarded from our dataset. A regression for normalized A_T ($NA_T = A_T \cdot 35/S$) was obtained from a NA_T vs. $[Si(OH)_4]$ (silicate concentration) scatter plot that included all valid A_T measurements in the dataset below 100 m depth, after Pérez et al. (2002). This practice is justified given the low variability of A_T in the North Atlantic (Friis et al., 2005), and yielded a satisfactory NA_T fit as a function of silicate concentration ($NA_T = 2294.7 + 1.37 \times [Si(OH)_4]$; $R^2 = 0.97$ and standard deviation of residuals of $\pm 3.7\,\mu mol\,kg^{-1}$). The obtained equation for the fit was then applied to the AR07E and A01E datasets to generate A_T values at the sampling depths of measured C_T.

3 Methodology

3.1 The $\varphi\, C_T^\circ$ method to calculate C_{ant} concentrations

The concentrations of C_{ant} shown in Fig. 2 (and in the rest of the cruises, not plotted) were estimated applying the φC_T° method (Pérez et al., 2008; Vázquez-Rodríguez et al., 2009a). The φC_T° method is a process-oriented geochemical approach that attempts to account for the nature and evolution of the phenomena that ultimately have affected oceanic C_{ant} storage since the 1750s. The method considers processes that control the uptake of C_{ant} by the ocean: from the biogeochemistry of the marine carbon cycle to the mixing and air-sea exchanges. It also considers the spatiotemporal variability of the A_T° and air-sea CO_2 disequilibrium (ΔC_{dis}) terms since the pre-industrial era. The subsurface layer reference for water mass formation conditions produced parameterizations of A_T° and ΔC_{dis} that serve to estimate C_{ant} without the need for any additional zero-C_{ant} references. A random propagation of the errors associated with the input variables necessary to calculate C_{ant} according to the φC_T° formulation yielded an overall uncertainty of $\pm 5.2\,\mu mol\,kg^{-1}$. This way of calculating uncertainties has been successfully used in the past by many authors (Gruber et al., 1996; Lee et al., 2003; Lo Monaco et al., 2005). The work from Vázquez-Rodríguez et al. (2009b) compared five independent estimation methodologies of C_{ant} in the Atlantic Ocean. According to this study, the φC_T° approach consistently yielded the closest values to the average of all five C_{ant} methodologies over the whole latitudinal range of the Atlantic. Appendix B2 further discusses the choice of the φC_T° method with respect to other methodologies, and a comparison of results is made with the TrOCA approach (Touratier et al., 2007).

3.2 On C_{ant} inventory estimation

The high convection activity and C_{ant} sequestration potential of the studied area, motivated a water mass approach to improve the accuracy of calculated inventories and storage rates. In practice, following a particular set of water masses and studying the temporal variability of their carbon system, has several advantages. Most importantly, this *modus operandi* treats the water masses that are present differently, in terms of their relative contributions to the column inventories of a tracer, unlike in closed volume, basin-wide approaches that treated all the water masses in the box equally. To avoid such caveats, we have identified the predominant water masses in the study area so that the variability of properties within each defined layer (Fig. 1b) is kept to a minimum (Table 2). Since the mixing between water masses still occurs, the observed changes in their properties over time can mainly be attributed to water mass formation conditions. This same strategy has been successfully used in the past by various authors (Azetsu-Scott et al., 2003; Kieke et al., 2007; Sarafanov et al., 2007; Pérez et al., 2008).

The limits, of the principal water masses in our study area, were identified in a TS diagram and then set to *ad hoc* isopycnals in the Irminger, Iceland and ENA basins (Fig. 1b; Table 2). For the sake of consistency, the potential density (σ, in $kg\,m^{-3}$) limits suggested in previous works (Kieke et al., 2007; Yashayaev et al., 2008) were adopted, whenever possible. Given that the spatial coverage of measurements is not optimum everywhere, this layer approach also allows for a better extrapolation of the observed water mass properties during a particular cruise to the rest of the basin. This water mass approach for improving inventory estimates makes evaluating the thickness variability of each layer possible,

Table 2a. Temporal evolution between 1981 and 2006 of the average ± standard error of the estimate ($\pm\sigma\Big/\sqrt{N}$, where N= number of data) salinity (S), potential temperature (θ), apparent oxygen utilization (AOU), silicate concentration ($[Si(OH)_4]$) and C_{ant} concentration for the water masses considered in the Irminger basin **(2a)**, the Iceland basin **(2b)** and the ENA basin **(2c)**. In the case of Thickness (Th), the standard deviation is given instead of the standard error of the estimate. The acronyms "l" and "c" stand for "layer" and "cruise", respectively. The "Obs." acronym in the second "Thickness" column stands for "observed" from cruise measurements. The WOA05 climatological values are given as references. The WOA05 value in the "Cruise-Year" column represents the climatological basin conditions calculated from WOA05 data (details given in Appendix A). Whenever a year is listed more than once it is because more than one cruise was conducted in this particular basin, for example, the 1997 cruises FOUREX and MET97 in the Irminger basin (Table 2a). All values listed here were obtained by vertically and horizontally integrating each property within each layer.

Cruise-Year	$Th^{WOA05}_{Irm,l,c}$ (m)	$Th^{obs}_{Irm,l,c}$ (m)	$F_{Irm,l,c}$	Salinity	θ (°C)	AOU ($\mu mol\,kg^{-1}$)	$[Si(OH)_4]$ ($\mu mol\,kg^{-1}$)	$C^{Irm,l,c}_{ant}$ ($\mu mol\,kg^{-1}$)
SAIW (σ_0<27.68 kg m^{-3})								
TTO – 81	497 ± 126	425 ± 116	0.79 ± 0.14	34.894 ± 0.002	5.370 ± 0.006	18.6 ± 0.3	7.96 ± 0.09	29.2 ± 1.5
AR07 – 91	496 ± 87	144 ± 161	0.28 ± 0.18	34.981 ± 0.002	5.228 ± 0.010	19.0 ± 0.5	8.50 ± 0.15	34.6 ± 2.5
A01E – 91	494 ± 71	303 ± 60	0.62 ± 0.06	34.962 ± 0.001	5.482 ± 0.004	25.8 ± 0.2	8.96 ± 0.05	35.2 ± 0.9
4x – 97	427 ± 67	468 ± 98	1.11 ± 0.12	34.911 ± 0.001	5.902 ± 0.005	27.9 ± 0.2	7.69 ± 0.07	38.7 ± 1.2
MET – 97	371 ± 43	414 ± 45	1.05 ± 0.06	34.893 ± 0.001	5.134 ± 0.003	30.1 ± 0.2	8.83 ± 0.05	38.9 ± 0.8
Ovide – 02	452 ± 47	405 ± 35	0.87 ± 0.04	34.949 ± 0.001	5.362 ± 0.004	24.6 ± 0.2	8.08 ± 0.06	41.1 ± 0.9
Ovide – 04	456 ± 44	556 ± 40	1.15 ± 0.04	34.967 ± 0.001	5.611 ± 0.003	23.8 ± 0.1	7.93 ± 0.04	44.2 ± 0.7
Ovide – 06	445 ± 36	564 ± 33	1.21 ± 0.04	34.977 ± 0.001	5.660 ± 0.003	24.1 ± 0.1	7.88 ± 0.04	44.1 ± 0.6
WOA05	*434 ± 12*	*	*	34.964 ± 0.004	5.544 ± 0.027	19.7 ± 0.3	7.89 ± 0.04	*
*u*LSW (27.68<σ_0<27.76 kg m^{-3})								
TTO – 81	555 ± 72	823 ± 102	1.37 ± 0.10	34.865 ± 0.001	3.534 ± 0.004	28.1 ± 0.2	9.28 ± 0.07	25.2 ± 1.1
AR07 – 91	581 ± 61	713 ± 78	1.18 ± 0.07	34.889 ± 0.001	3.577 ± 0.004	24.2 ± 0.2	9.52 ± 0.07	31.3 ± 1.1
A01E – 91	567 ± 41	616 ± 35	1.10 ± 0.04	34.900 ± 0.001	3.728 ± 0.003	28.7 ± 0.2	10.05 ± 0.05	28.4 ± 0.8
4x – 97	600 ± 37	515 ± 47	0.87 ± 0.04	34.877 ± 0.001	3.533 ± 0.005	35.6 ± 0.3	9.67 ± 0.08	31.2 ± 1.3
MET – 97	588 ± 33	506 ± 26	0.81 ± 0.02	34.869 ± 0.001	3.520 ± 0.003	35.9 ± 0.1	10.17 ± 0.04	32.8 ± 0.7
Ovide – 02	587 ± 34	686 ± 36	1.14 ± 0.03	34.896 ± 0.001	3.803 ± 0.003	35.0 ± 0.1	9.30 ± 0.04	32.7 ± 0.6
Ovide – 04	588 ± 36	673 ± 51	1.08 ± 0.03	34.888 ± 0.001	3.710 ± 0.003	37.2 ± 0.1	9.50 ± 0.04	33.1 ± 0.7
Ovide – 06	590 ± 39	637 ± 36	1.03 ± 0.03	34.902 ± 0.001	3.831 ± 0.002	34.4 ± 0.1	9.48 ± 0.04	35.0 ± 0.6
WOA05	*358 ± 17*	*	*	34.925 ± 0.002	3.997 ± 0.020	33.5 ± 0.2	9.62 ± 0.04	*
*c*LSW (27.6<σ_0<27.81 kg m^{-3})								
TTO – 81	875 ± 75	557 ± 63	0.59 ± 0.04	34.917 ± 0.002	3.375 ± 0.008	39.1 ± 0.4	10.58 ± 0.12	18.6 ± 2.0
AR07 - 91	747 ± 67	970 ± 94	1.25 ± 0.06	34.879 ± 0.001	3.137 ± 0.003	32.6 ± 0.2	10.16 ± 0.05	24.6 ± 0.8
A01E – 91	791 ± 71	869 ± 81	1.11 ± 0.05	34.881 ± 0.001	3.156 ± 0.003	29.8 ± 0.1	10.30 ± 0.04	25.6 ± 0.7
4x – 97	933 ± 98	988 ± 142	1.07 ± 0.07	34.871 ± 0.001	2.986 ± 0.004	31.1 ± 0.2	9.94 ± 0.06	29.7 ± 1.0
MET – 97	802 ± 67	983 ± 80	1.12 ± 0.04	34.868 ± 0.001	2.989 ± 0.003	30.9 ± 0.1	10.43 ± 0.04	29.9 ± 0.7
Ovide – 02	810 ± 30	678 ± 43	0.82 ± 0.02	34.897 ± 0.001	3.184 ± 0.003	38.8 ± 0.2	10.23 ± 0.05	26.2 ± 0.8
Ovide – 04	828 ± 28	546 ± 41	0.64 ± 0.02	34.902 ± 0.001	3.232 ± 0.004	40.5 ± 0.2	10.44 ± 0.06	27.7 ± 0.9
Ovide – 06	828 ± 28	535 ± 28	0.62 ± 0.01	34.923 ± 0.001	3.369 ± 0.003	40.8 ± 0.2	10.58 ± 0.05	27.8 ± 0.8
WOA05	*453 ± 25*	*	*	34.899 ± 0.001	3.314 ± 0.012	35.7 ± 0.1	10.25 ± 0.03	*
*u*NADW (27.81<σ_0<27.88 kg m^{-3})								
TTO – 81	466 ± 54	686 ± 104	1.35 ± 0.11	34.948 ± 0.001	2.980 ± 0.005	44.3 ± 0.2	12.01 ± 0.07	14.1 ± 1.2
AR07 – 91	498 ± 42	746 ± 82	1.44 ± 0.07	34.940 ± 0.001	2.925 ± 0.003	48.4 ± 0.2	12.66 ± 0.05	12.9 ± 0.8
A01E – 91	472 ± 54	667 ± 84	1.43 ± 0.08	34.935 ± 0.001	2.887 ± 0.003	44.9 ± 0.2	12.79 ± 0.05	15.3 ± 0.8
4x – 97	525 ± 63	516 ± 60	0.99 ± 0.07	34.917 ± 0.001	2.785 ± 0.005	41.5 ± 0.3	11.26 ± 0.08	20.0 ± 1.3
MET – 97	670 ± 58	754 ± 78	1.06 ± 0.06	34.924 ± 0.001	2.813 ± 0.004	44.2 ± 0.2	12.81 ± 0.06	20.0 ± 1.0
Ovide – 02	540 ± 54	762 ± 64	1.37 ± 0.06	34.918 ± 0.001	2.759 ± 0.003	43.7 ± 0.1	11.50 ± 0.04	19.7 ± 0.7
Ovide – 04	532 ± 59	755 ± 69	1.34 ± 0.06	34.916 ± 0.001	2.753 ± 0.003	44.4 ± 0.1	11.70 ± 0.04	22.6 ± 0.7
Ovide – 06	551 ± 55	745 ± 75	1.29 ± 0.06	34.930 ± 0.001	2.859 ± 0.003	43.2 ± 0.1	11.70 ± 0.04	23.0 ± 0.7
WOA05	*275 ± 9*	*	*	34.915 ± 0.003	2.869 ± 0.028	42.7 ± 0.2	11.30 ± 0.10	*
DSOW (σ_0>27.88 kg m^{-3})								
TTO – 81	47 ± 28	98 ± 28	1.92 ± 0.66	34.892 ± 0.002	1.679 ± 0.008	36.7 ± 0.4	9.80 ± 0.12	12.7 ± 2.0
AR07 – 91	105 ± 35	134 ± 35	1.22 ± 0.23	34.897 ± 0.001	1.778 ± 0.005	41.6 ± 0.3	10.20 ± 0.08	12.7 ± 1.4
A01E – 91	291 ± 24	86 ± 24	0.30 ± 0.04	34.896 ± 0.001	1.794 ± 0.006	38.1 ± 0.3	10.57 ± 0.09	15.5 ± 1.5
4x – 97	242 ± 36	90 ± 36	0.38 ± 0.09	34.897 ± 0.002	1.772 ± 0.009	38.0 ± 0.5	9.73 ± 0.14	20.5 ± 2.3
MET – 97	151 ± 28	94 ± 28	0.59 ± 0.11	34.894 ± 0.002	1.720 ± 0.008	38.8 ± 0.4	11.11 ± 0.13	20.1 ± 2.1
Ovide – 02	144 ± 21	110 ± 21	0.74 ± 0.08	34.887 ± 0.001	1.721 ± 0.005	39.4 ± 0.3	9.53 ± 0.08	17.7 ± 1.3
Ovide – 04	167 ± 26	112 ± 26	0.63 ± 0.07	34.869 ± 0.001	1.535 ± 0.005	36.3 ± 0.2	8.92 ± 0.07	21.9 ± 1.1
Ovide – 06	158 ± 31	126 ± 31	0.77 ± 0.10	34.906 ± 0.001	1.874 ± 0.004	37.7 ± 0.2	9.77 ± 0.07	22.4 ± 1.1
WOA05	*56 ± 123*	*	*	34.895 ± 0.004	1.885 ± 0.064	40.1 ± 0.2	11.08 ± 0.19	*

Table 2b. Iceland basin.

Cruise-Year	$Th^{WOA05}_{Ice,l,c}$ (m)	$Th^{obs}_{Ice,l,c}$ (m)	$F_{Ice,l,c}$	Salinity	θ (°C)	AOU (μmol kg^{-1})	[$Si(OH)_4$] (μmol kg^{-1})	$C^{Ice,l,c}_{ant}$ (μmol kg^{-1})
SAIW (σ_0 <27.60 kg m^{-3})								
TTO – 81	438 ± 61	445 ± 91	1.05 ± 0.12	35.183 ± 0.001	8.242 ± 0.003	28.2 ± 0.1	6.89 ± 0.04	25.8 ± 0.7
AR7E – 91	764 ± 56	694 ± 49	0.86 ± 0.04	35.109 ± 0.001	7.030 ± 0.003	22.9 ± 0.2	7.73 ± 0.05	34.4 ± 0.8
A01E – 91	974 ± 53	531 ± 35	0.91 ± 0.05	35.000 ± 0.002	6.935 ± 0.007	37.8 ± 0.3	8.94 ± 0.10	37.4 ± 1.7
OACES – 93	691 ± 23	840 ± 36	1.12 ± 0.03	35.151 ± 0.001	7.889 ± 0.003	31.6 ± 0.1	6.68 ± 0.04	39.7 ± 0.7
4x – 97	475 ± 31	535 ± 41	1.13 ± 0.05	35.094 ± 0.001	7.931 ± 0.003	47.2 ± 0.2	8.17 ± 0.05	39.5 ± 0.8
CHAOS – 98	668 ± 25	864 ± 30	1.19 ± 0.03	35.249 ± 0.001	8.563 ± 0.003	28.7 ± 0.2	7.22 ± 0.05	41.1 ± 0.8
Ovide – 02	619 ± 22	647 ± 38	1.10 ± 0.04	35.117 ± 0.001	7.614 ± 0.003	30.5 ± 0.2	7.33 ± 0.05	42.2 ± 0.8
A16N – 03	729 ± 33	803 ± 31	0.93 ± 0.02	35.260 ± 0.001	8.826 ± 0.002	37.4 ± 0.1	6.68 ± 0.03	44.3 ± 0.5
Ovide – 04	618 ± 18	555 ± 17	0.97 ± 0.02	35.105 ± 0.001	7.719 ± 0.002	38.5 ± 0.1	7.40 ± 0.04	43.5 ± 0.6
Ovide – 06	629 ± 21	576 ± 22	0.97 ± 0.02	35.077 ± 0.001	7.906 ± 0.003	38.7 ± 0.1	7.20 ± 0.04	44.2 ± 0.7
WOA05	*636 ± 13*	*	*	35.175 ± 0.002	7.954 ± 0.027	29.6 ± 0.4	7.36 ± 0.04	*
*u*LSW (σ_0>27.60 kg m^{-3};σ_1<32.35 kg m^{-3})								
TTO – 81	868 ± 78	535 ± 59	0.63 ± 0.05	34.982 ± 0.001	4.637 ± 0.005	48.5 ± 0.3	10.56 ± 0.08	19.1 ± 1.3
AR7E – 91	548 ± 27	602 ± 21	1.04 ± 0.03	34.959 ± 0.001	4.488 ± 0.004	56.2 ± 0.2	10.87 ± 0.06	21.1 ± 0.9
A01E – 91	767 ± 34	559 ± 24	1.22 ± 0.05	34.944 ± 0.001	4.340 ± 0.006	51.7 ± 0.3	11.16 ± 0.09	23.0 ± 1.5
OACES – 93	581 ± 25	463 ± 15	0.74 ± 0.02	34.987 ± 0.001	4.754 ± 0.004	56.0 ± 0.2	10.43 ± 0.06	23.2 ± 1.1
4x – 97	549 ± 32	472 ± 26	0.87 ± 0.03	34.940 ± 0.001	4.345 ± 0.003	55.7 ± 0.2	11.11 ± 0.05	27.2 ± 0.8
CHAOS – 98	618 ± 23	479 ± 27	0.71 ± 0.03	35.009 ± 0.002	4.938 ± 0.007	62.2 ± 0.3	11.72 ± 0.10	24.2 ± 1.7
Ovide – 02	508 ± 22	512 ± 24	1.06 ± 0.03	34.976 ± 0.001	4.657 ± 0.003	57.5 ± 0.2	10.60 ± 0.05	25.3 ± 0.9
A16N – 03	455 ± 37	512 ± 43	0.95 ± 0.06	35.024 ± 0.001	4.979 ± 0.004	63.7 ± 0.2	11.24 ± 0.06	26.0 ± 1.0
Ovide – 04	504 ± 24	595 ± 40	1.27 ± 0.04	34.948 ± 0.001	4.408 ± 0.002	55.7 ± 0.1	10.68 ± 0.04	27.9 ± 0.6
Ovide – 06	506 ± 22	568 ± 21	1.19 ± 0.03	34.956 ± 0.001	4.494 ± 0.003	54.4 ± 0.1	10.74 ± 0.04	30.3 ± 0.7
WOA05	*360 ± 14*	*	*	35.015 ± 0.002	4.924 ± 0.001	54.1 ± 0.3	10.79 ± 0.05	*
*c*LSW (σ_1 >32.35 kg m^{-3}; σ_2 <37.00 kg m^{-3})								
TTO – 81	632 ± 113	650 ± 136	1.05 ± 0.17	34.943 ± 0.001	3.517 ± 0.004	44.7 ± 0.2	12.13 ± 0.07	17.2 ± 1.1
AR7E – 91	784 ± 78	826 ± 68	0.99 ± 0.06	34.928 ± 0.001	3.376 ± 0.003	45.6 ± 0.1	11.59 ± 0.04	15.8 ± 0.7
A01E – 91	1879 ± 157	1038 ± 127	0.92 ± 0.08	34.923 ± 0.001	3.308 ± 0.005	43.5 ± 0.3	12.31 ± 0.08	18.9 ± 1.3
OACES – 93	400 ± 114	454 ± 124	1.05 ± 0.25	34.926 ± 0.001	3.458 ± 0.005	44.6 ± 0.2	11.27 ± 0.07	20.4 ± 1.2
4x – 97	1324 ± 67	1302 ± 72	0.99 ± 0.03	34.905 ± 0.001	3.170 ± 0.002	40.1 ± 0.1	11.72 ± 0.04	23.4 ± 0.6
CHAOS – 98	326 ± 98	411 ± 138	1.16 ± 0.34	34.919 ± 0.002	3.372 ± 0.006	44.1 ± 0.3	12.08 ± 0.09	26.0 ± 1.6
Ovide – 02	1139 ± 121	919 ± 97	0.85 ± 0.06	34.920 ± 0.001	3.273 ± 0.003	43.1 ± 0.1	11.06 ± 0.04	23.5 ± 0.7
A16N – 03	361 ± 88	446 ± 118	1.04 ± 0.23	34.926 ± 0.001	3.387 ± 0.005	45.2 ± 0.3	11.79 ± 0.08	27.1 ± 1.3
Ovide – 04	1164 ± 65	971 ± 58	0.90 ± 0.03	34.909 ± 0.001	3.226 ± 0.003	43.8 ± 0.1	11.32 ± 0.04	24.7 ± 0.6
Ovide – 06	1179 ± 76	1001 ± 70	0.90 ± 0.04	34.919 ± 0.001	3.297 ± 0.003	42.2 ± 0.1	11.39 ± 0.04	26.9 ± 0.6
WOA05	*529 ± 23*	*	*	34.936 ± 0.001	3.414 ± 0.012	45.1 ± 0.1	11.67 ± 0.05	*
*u*NADW (σ_2 >37.00 kg m^{-3}; σ_4 <45.84 kg m^{-3})								
TTO – 81	159 ± 68	236 ± 86	1.52 ± 0.58	34.970 ± 0.002	2.732 ± 0.007	52.9 ± 0.3	10.74 ± 0.10	10.7 ± 1.7
AR7E – 91	199 ± 26	328 ± 37	1.55 ± 0.14	34.972 ± 0.001	2.762 ± 0.004	53.0 ± 0.2	14.66 ± 0.05	12.6 ± 0.9
A01E – 91	760 ± 147	505 ± 157	1.11 ± 0.23	34.963 ± 0.001	2.718 ± 0.005	55.2 ± 0.2	18.44 ± 0.07	13.3 ± 1.2
OACES – 93	86 ± 32	87 ± 22	0.93 ± 0.36	34.971 ± 0.003	2.816 ± 0.012	49.3 ± 0.6	12.95 ± 0.18	15.5 ± 3.1
4x – 97	690 ± 76	537 ± 66	0.78 ± 0.07	34.949 ± 0.001	2.689 ± 0.004	50.0 ± 0.2	15.53 ± 0.06	17.2 ± 1.0
CHAOS – 98	150 ± 85	55 ± 55	0.34 ± 0.38	34.967 ± 0.004	2.749 ± 0.017	49.7 ± 0.9	13.69 ± 0.26	19.5 ± 4.4
Ovide – 02	459 ± 45	426 ± 36	0.97 ± 0.07	34.964 ± 0.001	2.704 ± 0.004	52.8 ± 0.2	15.52 ± 0.05	17.9 ± 0.9
A16N – 03	72 ± 56	113 ± 65	1.31 ± 1.09	34.975 ± 0.003	2.833 ± 0.012	48.3 ± 0.6	13.51 ± 0.18	23.8 ± 3.1
Ovide – 04	430 ± 67	339 ± 67	0.85 ± 0.11	34.959 ± 0.001	2.675 ± 0.004	56.0 ± 0.2	17.09 ± 0.06	17.1 ± 1.0
Ovide – 06	479 ± 15	469 ± 15	1.04 ± 0.02	34.964 ± 0.001	2.705 ± 0.003	53.2 ± 0.2	17.54 ± 0.05	19.7 ± 0.8
WOA05	*149 ± 15*	*	*	34.963 ± 0.004	2.710 ± 0.025	56.5 ± 0.3	18.77 ± 0.77	*

Table 2c. Eastern North Atlantic Basin

Cruise-Year	$Th^{obs}_{ENA,l,c}$ (m)	Salinity	θ (°C)	AOU ($\mu mol\,kg^{-1}$)	$[Si(OH)_4]$ ($\mu mol\,kg^{-1}$)	$C^{ENA,l,c}_{ant}$ ($\mu mol\,kg^{-1}$)	$^{*}C^{ENA,l,c}_{ant}$ ($\mu mol\,kg^{-1}$)
NACW (σ_0<27.20 kg m^{-3})							
TTO – 81	459 ± 33	35.618 ± 0.001	12.472 ± 0.003	27.5 ± 0.2	3.74 ± 0.05	34.6 ± 0.9	34.6 ± 0.9
BD3 – 89	439 ± 88	35.661 ± 0.001	12.448 ± 0.004	23.6 ± 0.2	2.86 ± 0.06	38.5 ± 1.0	38.5 ± 1.0
TYRO – 90	454 ± 53	35.668 ± 0.001	12.160 ± 0.003	19.7 ± 0.1	3.52 ± 0.04	41.3 ± 0.7	41.3 ± 0.7
A01E – 91	334 ± 25	35.532 ± 0.004	11.163 ± 0.015	22.5 ± 0.8	4.66 ± 0.23	43.1 ± 3.8	43.1 ± 3.8
OACES – 93	436 ± 26	35.544 ± 0.001	11.500 ± 0.004	23.0 ± 0.2	3.02 ± 0.07	44.7 ± 1.1	44.7 ± 1.1
4x – 97	495 ± 12	35.673 ± 0.000	12.375 ± 0.002	31.6 ± 0.1	3.58 ± 0.03	48.1 ± 0.5	48.1 ± 0.5
CHAOS – 98	470 ± 23	35.659 ± 0.001	12.293 ± 0.002	20.9 ± 0.1	3.62 ± 0.03	46.8 ± 0.5	46.8 ± 0.5
Ovide – 02	456 ± 21	35.643 ± 0.000	12.170 ± 0.002	26.1 ± 0.1	3.58 ± 0.03	51.3 ± 0.5	51.3 ± 0.5
A16N – 03	457 ± 27	35.657 ± 0.000	12.492 ± 0.002	25.1 ± 0.1	3.47 ± 0.03	52.0 ± 0.5	52.0 ± 0.5
Ovide – 04	463 ± 11	35.637 ± 0.000	12.116 ± 0.002	28.5 ± 0.1	3.63 ± 0.03	51.7 ± 0.5	51.7 ± 0.5
Ovide – 06	455 ± 10	35.659 ± 0.000	12.146 ± 0.002	24.1 ± 0.1	3.43 ± 0.03	56.2 ± 0.5	56.2 ± 0.5
WOA05	*256 ± 5*	35.552 ± 0.004	11.832 ± 0.029	17.9 ± 0.3	3.47 ± 0.02	*	*
MW (σ_0>27.20 kg m^{-3}; σ_1<32.35 kg m^{-3})							
TTO – 81	837 ± 47	35.408 ± 0.001	7.812 ± 0.003	72.4 ± 0.1	10.29 ± 0.04	24.4 ± 0.7	28.0 ± 0.9
BD3 – 89	1026 ± 22	35.745 ± 0.001	9.679 ± 0.003	74.4 ± 0.2	9.34 ± 0.05	31.4 ± 0.8	30.0 ± 1.0
TYRO – 90	1083 ± 77	35.250 ± 0.001	7.156 ± 0.004	64.2 ± 0.2	10.07 ± 0.05	27.2 ± 0.9	31.0 ± 1.1
A01E – 91	739 ± 71	35.107 ± 0.001	6.650 ± 0.003	54.1 ± 0.2	10.07 ± 0.05	28.0 ± 0.9	30.9 ± 1.2
OACES – 93	1068 ± 34	35.242 ± 0.001	7.125 ± 0.003	64.9 ± 0.1	9.08 ± 0.04	27.9 ± 0.7	32.0 ± 0.9
4x – 97	944 ± 18	35.509 ± 0.000	8.413 ± 0.002	75.4 ± 0.1	9.77 ± 0.02	30.7 ± 0.4	33.6 ± 0.7
CHAOS – 98	1020 ± 32	35.323 ± 0.001	7.542 ± 0.003	74.6 ± 0.2	10.46 ± 0.05	27.2 ± 0.8	33.0 ± 1.1
Ovide – 02	952 ± 13	35.490 ± 0.000	8.262 ± 0.001	74.2 ± 0.1	9.66 ± 0.02	31.4 ± 0.4	34.2 ± 0.6
A16N – 03	1050 ± 15	35.365 ± 0.001	7.771 ± 0.002	78.5 ± 0.1	10.21 ± 0.03	28.2 ± 0.6	34.4 ± 0.9
Ovide – 04	947 ± 15	35.456 ± 0.000	8.038 ± 0.001	75.2 ± 0.1	9.86 ± 0.02	31.0 ± 0.4	34.7 ± 0.7
Ovide – 06	967 ± 13	35.493 ± 0.000	8.218 ± 0.001	75.1 ± 0.1	9.76 ± 0.02	34.0 ± 0.4	37.0 ± 0.7
WOA05	*791 ± 15*	35.395 ± 0.004	8.176 ± 0.037	60.2 ± 0.7	9.28 ± 0.05	*	*
LSW (σ_1>32.35 kg m^{-3}; σ_2<37.00 kg m^{-3})							
TTO – 81	884 ± 78	35.057 ± 0.001	3.975 ± 0.004	56.0 ± 0.2	15.15 ± 0.06	14.4 ± 1.0	12.5 ± 1.3
BD3 – 89	565 ± 49	35.107 ± 0.001	4.353 ± 0.006	62.7 ± 0.3	16.90 ± 0.09	17.7 ± 1.5	15.6 ± 1.8
TYRO – 90	1123 ± 116	35.002 ± 0.002	3.712 ± 0.006	54.5 ± 0.3	14.41 ± 0.10	16.9 ± 1.6	16.2 ± 1.7
A01E – 91	960 ± 37	34.920 ± 0.001	3.286 ± 0.004	45.4 ± 0.2	13.21 ± 0.06	17.3 ± 1.0	16.2 ± 1.1
OACES – 93	1082 ± 58	34.946 ± 0.001	3.422 ± 0.004	47.2 ± 0.2	12.33 ± 0.05	18.6 ± 0.9	17.3 ± 1.1
4x – 97	985 ± 31	34.997 ± 0.001	3.673 ± 0.002	55.0 ± 0.1	15.27 ± 0.03	20.1 ± 0.6	19.9 ± 0.7
CHAOS – 98	1220 ± 63	34.962 ± 0.001	3.515 ± 0.004	50.2 ± 0.2	13.94 ± 0.05	20.6 ± 0.9	19.7 ± 1.1
Ovide – 02	1192 ± 25	34.990 ± 0.000	3.636 ± 0.002	51.9 ± 0.1	14.01 ± 0.03	20.6 ± 0.4	19.5 ± 0.6
A16N – 03	1200 ± 45	34.957 ± 0.001	3.466 ± 0.003	52.6 ± 0.2	13.60 ± 0.05	18.9 ± 0.8	19.3 ± 0.9
Ovide – 04	1175 ± 21	34.986 ± 0.000	3.606 ± 0.002	53.0 ± 0.1	14.01 ± 0.02	21.1 ± 0.4	20.6 ± 0.6
Ovide – 06	1151 ± 24	34.989 ± 0.000	3.642 ± 0.002	50.7 ± 0.1	13.54 ± 0.03	23.6 ± 0.4	22.1 ± 0.6
WOA05	*511 ± 22*	34.990 ± 0.005	3.673 ± 0.031	55.4 ± 0.4	14.99 ± 0.13	*	*
*u*NADW (σ_2>37.00 kg m^{-3}; σ_4<45.84 kg m^{-3})							
TTO – 81	731 ± 144	34.947 ± 0.001	2.610 ± 0.005	71.7 ± 0.2	30.40 ± 0.07	7.8 ± 1.2	7.1 ± 1.3
BD3 – 89	1072 ± 220	34.959 ± 0.001	2.738 ± 0.005	74.7 ± 0.3	31.98 ± 0.08	9.7 ± 1.3	9.3 ± 1.5
TYRO – 90	1018 ± 128	34.947 ± 0.002	2.571 ± 0.009	75.9 ± 0.5	32.14 ± 0.14	12.5 ± 2.3	9.8 ± 2.7
A01E – 91	513 ± 86	34.943 ± 0.001	2.574 ± 0.004	68.5 ± 0.2	28.34 ± 0.06	9.1 ± 1.1	9.2 ± 1.1
OACES – 93	929 ± 55	34.945 ± 0.001	2.585 ± 0.006	69.4 ± 0.3	28.53 ± 0.08	9.7 ± 1.4	8.9 ± 1.5
4x – 97	831 ± 64	34.944 ± 0.001	2.597 ± 0.003	76.3 ± 0.1	32.62 ± 0.04	8.0 ± 0.7	8.7 ± 0.8
CHAOS – 98	934 ± 67	34.941 ± 0.001	2.564 ± 0.005	72.6 ± 0.2	31.22 ± 0.07	9.7 ± 1.2	10.8 ± 1.4
Ovide – 02	1072 ± 30	34.948 ± 0.000	2.611 ± 0.002	71.9 ± 0.1	30.97 ± 0.03	10.0 ± 0.4	9.1 ± 0.6
A16N – 03	973 ± 89	34.938 ± 0.001	2.515 ± 0.005	77.3 ± 0.2	31.52 ± 0.07	10.1 ± 1.2	10.2 ± 1.2
Ovide – 04	1111 ± 25	34.943 ± 0.000	2.588 ± 0.002	73.8 ± 0.1	31.17 ± 0.03	9.8 ± 0.4	11.0 ± 0.7
Ovide – 06	1100 ± 31	34.950 ± 0.000	2.626 ± 0.002	70.5 ± 0.1	30.81 ± 0.03	11.8 ± 0.5	10.8 ± 0.6
WOA05	*549 ± 28*	34.944 ± 0.001	2.589 ± 0.013	77.9 ± 0.2	33.02 ± 0.32	*	*
*l*NADW (σ_4>45.84 kg m^{-3})							
TTO – 81	285 ± 156	34.907 ± 0.001	2.151 ± 0.006	85.2 ± 0.3	43.67 ± 0.09	5.9 ± 1.5	4.1 ± 1.6
BD3 – 89	640 ± 150	34.905 ± 0.001	2.130 ± 0.005	85.2 ± 0.3	44.98 ± 0.08	8.5 ± 1.3	6.7 ± 1.4
TYRO – 90	879 ± 135	34.909 ± 0.002	1.964 ± 0.009	90.3 ± 0.4	44.37 ± 0.13	5.0 ± 2.2	5.8 ± 2.3
A01E – 91	77 ± 91	34.910 ± 0.002	2.182 ± 0.008	87.5 ± 0.4	44.53 ± 0.11	5.8 ± 1.9	5.2 ± 2.0
OACES – 93	659 ± 72	34.915 ± 0.001	2.193 ± 0.005	84.5 ± 0.3	42.31 ± 0.08	7.0 ± 1.4	4.8 ± 1.7
4x 97	424 ± 113	34.904 ± 0.001	2.131 ± 0.003	87.4 ± 0.2	44.33 ± 0.05	3.6 ± 0.8	2.9 ± 0.9
CHAOS – 98	539 ± 98	34.911 ± 0.001	2.180 ± 0.005	87.0 ± 0.2	43.98 ± 0.07	6.5 ± 1.2	5.6 ± 1.3
Ovide – 02	566 ± 45	34.911 ± 0.001	2.158 ± 0.002	86.0 ± 0.1	44.54 ± 0.03	6.6 ± 0.5	5.1 ± 0.7
A16N – 03	548 ± 132	34.912 ± 0.001	2.192 ± 0.005	85.6 ± 0.2	42.05 ± 0.07	7.9 ± 1.2	6.2 ± 1.4
Ovide – 04	618 ± 67	34.906 ± 0.001	2.149 ± 0.002	87.0 ± 0.1	44.12 ± 0.03	5.8 ± 0.5	4.9 ± 0.7
Ovide – 06	581 ± 73	34.914 ± 0.001	2.159 ± 0.002	85.2 ± 0.1	45.53 ± 0.03	7.2 ± 0.6	5.4 ± 0.8
WOA05	*321 ± 17*	34.908 ± 0.001	2.101 ± 0.046	88.7 ± 0.5	42.96 ± 0.63	*	*

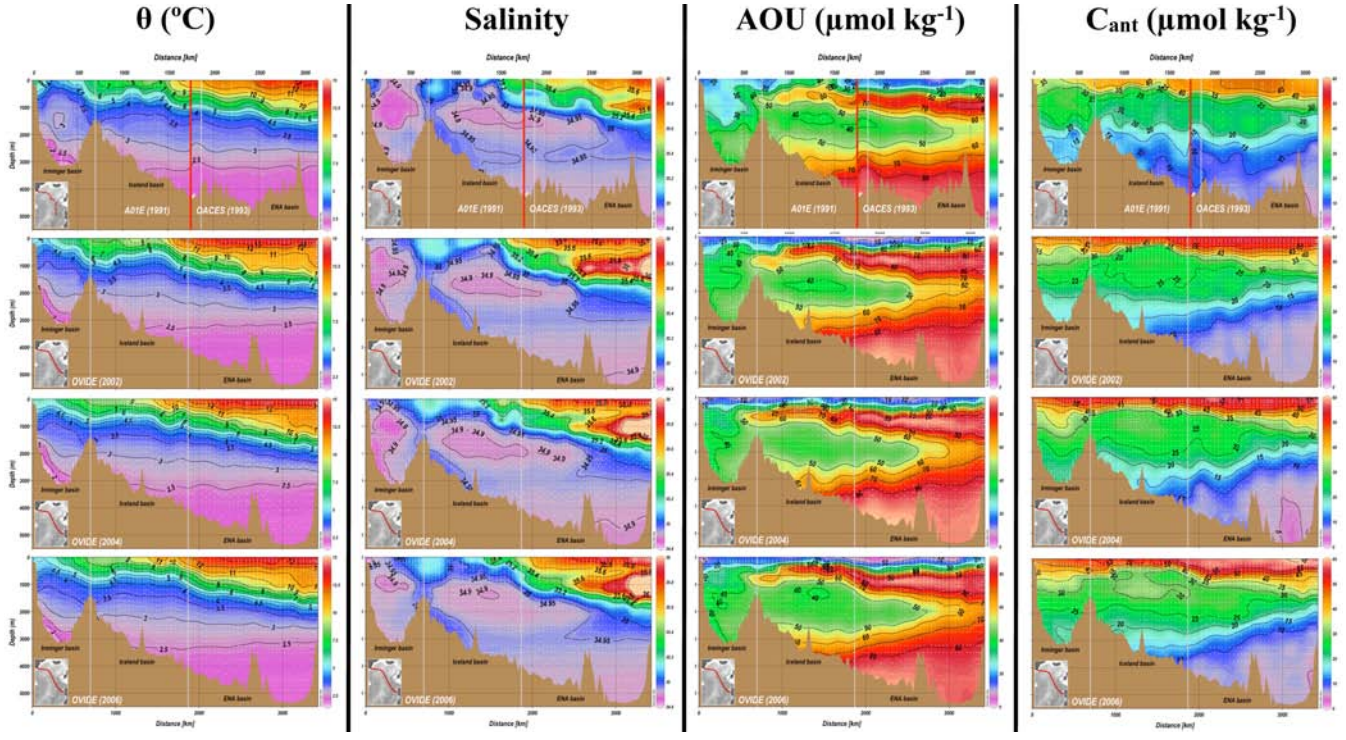

Fig. 2. Contour plots of θ, Salinity (S), AOU and C_{ant} concentration spanning from 1991 to 2006. The x-axis gives the track distances (km) from the southernmost tip of Greenland towards the Iberian Basin. The small white dots in each sub-plot indicate bottle depths and the grey vertical lines demarcate basin separations. The top row section is a composite from the A01E (1991) and OACES (1993) cruises (separated by thick red vertical line), in order to get the closest match possible with the OVIDE section. Notice that the selected A01E leg perfectly overlaps with the OVIDE tracks. This was done in order to extend directly comparable measurements and C_{ant} estimates of the OVIDE project further back in time by nearly a decade and get a better track of the storage trends. Compared with the nine-year gap between this composite section and the first OVIDE cruise in 2002, the temporal difference between the A01E and OACES cruises is negligible and affordable. On the top composite sections, the continuum fields at the insertion point of the upper, intermediate and deep waters corroborate this assumption and validate the combination of results.

which is much more realistic and representative of the hydrodynamics in our study area.

A few considerations are now made on how C_{ant} inventory and storage rates calculations were done in previous studies. The classical way to calculate inventories requires vertically integrating the C_{ant} concentrations over the entire water column of the considered area. If a transient steady state (Keeling and Bolin, 1967) is assumed for C_{ant} (Tanhua et al., 2006), then the mean penetration depth (MPD) can be defined as the quotient between the specific inventory of C_{ant} in the water column and the C_{ant} concentration in the winter mixed layer. The works from Holfort et al. (1998), Roson et al. (2003) or Álvarez et al. (2003) have approximated the C_{ant} storage rates as the product of the time derivative of the average C_{ant} concentration in the winter mixed layer ($\partial C_{ant}^{WML} / \partial t$) times the MPD. The basis for this approximation relies on the fact that MPD is taken as constant, after the work from Broecker et al. (1979). However, Pérez et al. (2008) pointed out that the time variability of the MPD could notoriously affect the estimates of C_{ant} storage rates, especially during high NAO periods in or close to areas of water mass formation.

The latter approximation of a constant MPD basically does not contemplate the changes in the volumetric census of the water masses caused by differential formation rates in different years, which has been shown to be particularly the case in the Irminger and Iceland basins (Fig. 2). The deviations from the assumption of constant MPDs propagate then into the inventory estimates, adding larger uncertainties and biases to them. The works from Kieke et al. (2006) and Steinfeldt et al. (2009), which calculated CFC inventories in the North Atlantic, had both pointed out the importance of considering the variability of water mass volumetric census for inventory calculation purposes. They showed that the detected changes in the CFC inventories were largely produced by the changes in layer thickness of *u*LSW and *c*LSW and not by actual changes in the concentrations.

To improve the accuracy of C_{ant} inventories, it is necessary to contemplate not only the changes in the C_{ant} concentrations, but also how the changes in the volumetric census of each water mass affect the column inventory of C_{ant}. To follow the variability of water mass formation, we have considered the variability of the layer thicknesses (*Th* hereinafter) for the water masses (Fig. 1b). In so doing, the need

for considering unrealistic constant MPDs throughout the entire basin can be avoided. The *Th* has been calculated as the average vertical distance between layers, weighed by the separation between stations. Also, the averages for potential temperature (θ), salinity (S), apparent oxygen utilization (AOU), [$Si(OH)_4$] and C_{ant} concentration were computed integrating vertically and horizontally, i.e., using the upper and lower layer boundaries (vertical integration), the lateral ends of the layers in each of the cruise tracks and within each of the basins (horizontal integration) and then dividing by the section area of the corresponding layer (Pérez et al., 2008). These average thicknesses and layer properties are listed in Table 2.

The inventory of C_{ant} for a given basin "b" calculated from the data of cruise "c" is formally defined as:

$$I_{b,c}^{C_{ant}} = \sum_{l=1}^{k} \rho_{b,l,c} \cdot C_{ant}^{b,l,c} \cdot Th_{b,l,c}^{*} \quad (1)$$

where the index "k" is the total number of layers found in each basin "b" (Fig. 1b), $C_{ant}^{b,l,c}$ (Table 2) stands for the average concentration of C_{ant} of layer "l" in basin "b" during cruise "c" (Table 2) and "ρ" is the seawater density (in kg m^{-3}). The $Th_{b,l,c}^{*}$ term in (1) is the thickness of layer "l" in basin "b" calculated by considering the actual thickness observed under the track of cruise "c" and extrapolating it to the rest of basin "b" (see Appendix A1). For this, we compared each *Th* calculated from cruise data (denoted as "*Th* observed" in Table 2) with the thickness calculated from climatological WOA05 data ("*Th* WOA05" in Table 2) for the same "l","b" and "c". The calculation minutiae for the $Th_{b,l,c}^{*}$ term in (1) are provided in Appendix A1.

Equation (1) has been applied in this study to calculate the inventories of C_{ant} in the Irminger and Iceland basins ("b=Irm" and "b=Ice"). The procedure to obtain more accurate inventory estimates for the ENA basin is slightly different (Eq. 2). The weaker convection in this region makes the layer thickness variability less important compared to the Irminger and Iceland basins. Also, due to its larger extension and the sparseness of measurements, the calculation of $Th_{b,l,c}^{*}$ in the ENA basin is not applied, i.e., in this case $Th_{ENA,l,c} = Th_{ENA,l}^{WOA05}$.

In addition, the large separation between cruises in the ENA basin and the actual spatial variability of the considered tracers can cause significant differences between the observed average layer properties in each cruise and those from mean basin values. Such differences are likely to introduce potential spatial biases in C_{ant} estimates. These differences can be corrected by considering the co-variances of C_{ant} in each layer with the water mass thermohaline properties (θ and S), and the state of ventilation (for which AOU is used as a proxy). For this, we assume that the deviations of these properties for each cruise, compared to the WOA05 basin average, can account for the *spatial* biases of C_{ant} estimates. Accordingly, the "C_{ant}^{ENA},l,c" terms in Eq. (1) are optimised

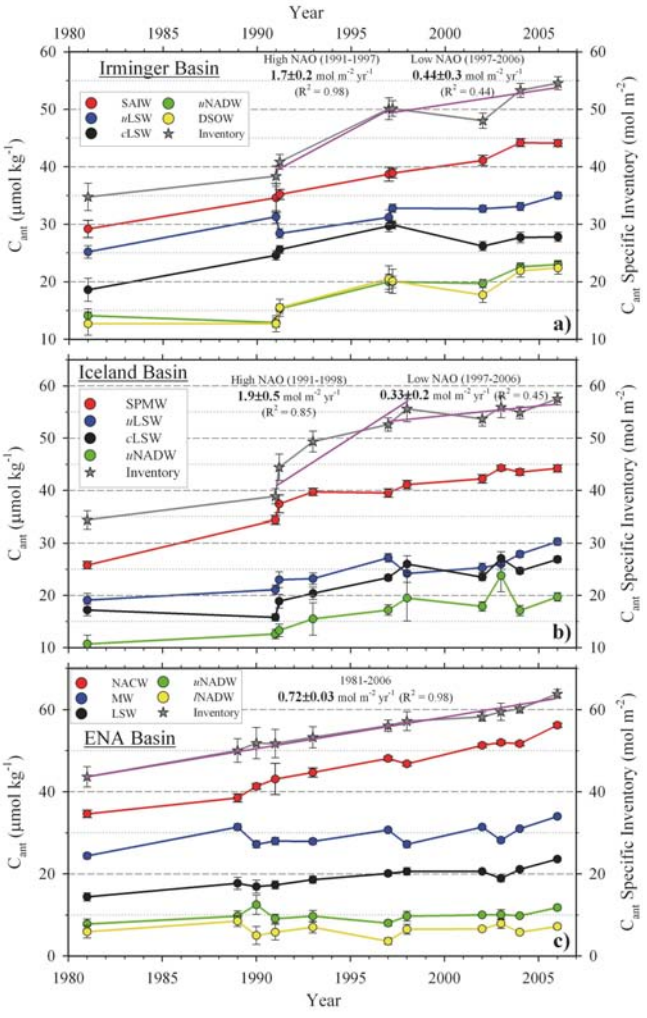

Fig. 3. Trends of average C_{ant} concentrations in the studied water masses at the Irminger (3a), Iceland (3b) and ENA (3c; $^{*}C_{ant}^{ENA,l,c}$ plotted) basins. Notice that the y-axis scale is *ad hoc* for each graph. The grey lines give the specific inventories and the purple fit lines stand for the rates of change of the specific inventories (slope and R^2 given for the high and low NAO index periods, except for the ENA basin). The error bars represent the standard error of the mean.

($^{*}C_{ant}^{ENA,l,c}$) by adding to them a new term "$\Delta C_{ant}^{ENA,l,c}$". The latter term represents the deviation of "$C_{ant}^{ENA,l,c}$" values (calculated from cruise data) from the *spatial* mean of C_{ant} in the ENA, which are calculated using θ, S and AOU data from WOA05. The calculation details are given in Appendix A2. The calculated values for both "$C_{ant}^{ENA,l,c}$" and "$\Delta C_{ant}^{ENA,l,c}$" are listed in Table 2c. Consequently, the calculation of C_{ant} inventories in the ENA basin is done by applying a slightly modified version of Eq. (1), namely:

$$I_{ENA,c}^{C_{ant}} = \sum_{l=1}^{k} \rho_{b,l,c} \cdot {}^{*}C_{ant}^{ENA,l,c} \cdot Th_{b,l}^{WOA05} \quad (2)$$

4 Results and discussion

The temporal trends of $C_{ant}^{Irminger,l,c}$, $C_{ant}^{Iceland,l,c}$ and ${}^{*}C_{ant}^{ENA,l,c}$ concentration averages for 1981–2006 (Table 2) are plotted in Fig. 3 together with the temporal trends of C_{ant} specific inventories, which were calculated as described in Sect. 3 from Eq. (1) and (2). The C_{ant} storage rates in each basin were calculated by considering the areas of the three basins given in Fig. 4. Since this was done over the entire study time period, the changes in the C_{ant} storage rates per basin and for the NASPG (the "OVIDE box"; Fig. 4) can be obtained and compared with the high and low NAO periods. These calculations and the specific inventory rates (purple lines in Fig. 3) are summarised in Table 3 and discussed below. An evaluation of the uncertainties associated with C_{ant} inventory calculations and the results shown in Table 3 is given in Appendix B1. Also, Appendix B2 discusses the choice of the φC_T° method and shows how the obtained results for C_{ant} storage rates are actually independent of the C_{ant} estimation approach used.

4.1 Evolution through 1981–2006 of the average C_{ant} concentrations in the NASPG water masses.

The C_{ant} concentrations (Fig. 2) generally increase over time in the upper layers (SAIW, SMPW and NACW) of the three basins considered. They evolve from average values of 35–40 µmol kg^{-1} in 1991–1993 to the peak average values (above 55 µmol kg^{-1}) recorded during the OVIDE 2006 cruise (Fig. 3). This result was anticipated by the increasing atmospheric xCO_2 over time, which went from ∼350 ppm in 1991 to ∼379 ppm in 2006. The C_{ant} isopleth of 15–20 µmol kg^{-1} demarcates a sharp gradient that separates more ventilated waters (formed originally in the North Atlantic) that have high C_{ant} concentrations from deeper waters coming from the south, with lower loads of C_{ant}. These deep waters have silicate values typically above 12 µmol kg^{-1} that trace the Antarctic influence. This C_{ant} isopleth deepens over time (Fig. 2), indicating a larger entrainment of C_{ant} towards the ocean interior. The increasing of C_{ant} during 1991–1997 in intermediate layers (particularly in LSW) is the result of the high convective activity of the North Atlantic. Conversely, the deeper water masses of the ENA basin (mostly *l*NADW) show no significant tendencies in their C_{ant} content between 1991 and 2006.

The speed with which the influence of the NAO is transmitted into the properties of the various water masses varies. These "reaction times" can generally be established in less than 3 years for the water masses in the Irminger basin and about 5 years for upper and intermediate waters in the Iceland basin. According to the latest estimates, the salinity minimum of *c*LSW is transmitted to the Irminger Sea in 2-years time during high-NAO periods and 2.5 years during weak convection periods (Pickart et al., 2003; Yashayaev et al., 2007; Thierry et al., 2008). Also, Yashayaev et al. (2008) suggest that it takes approximately 5 years for LSW to reach the Iceland basin. According to Johnson and Gruber (2007) and Thierry et al. (2008), the NAO leads by 2–3 years with the water mass properties of SPMW, mainly due to NAO wind-driven changes in circulation and advection. Regarding the SAIW, Sarafanov et al. (2008) have pointed out that the recent increase in salinity of the intermediate waters is the result of the contraction of the subpolar gyre following the 1996 NAO drop that causes the northward advance of the subtropical water masses. The strong correlations between the salinity values of intermediate waters and the 5-year running mean of the NAO index suggest that there exists a 2-year lag between the two phenomena (Sarafanov et al., 2008).

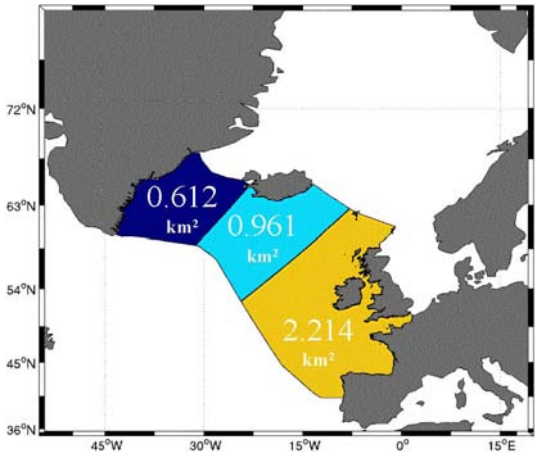

Fig. 4. Areas (in 10^6 km^2) of the Irminger (dark blue), Iceland (indigo blue) and ENA (yellow) basins enclosed by the "OVIDE box". These areas were used in the calculation of C_{ant} storage rates from the specific inventory estimates in Fig. 3. The northern geographical boundaries of the "OVIDE box" are defined by the North Atlantic sills east and west from Iceland (according to the ETOPO2 bathymethry), while the southern one is delimited by the tracks of the OVIDE cruises.

The enhanced production of LSW fostered a fast injection of C_{ant} into the upper and intermediate layers of the Irminger basin between 1981 and 1997. Although C_{ant} is seen to increase progressively from 1981 through 2006, this does not happen at a steady rate. The trend of rapid C_{ant} increase in the LSW layers of the Irminger observed during 1991–1997 (0.77 ± 0.07 µmol kg^{-1} yr^{-1}) clearly slows down during the OVIDE era (Table 2a, Fig. 3a), in agreement with the results in Pérez et al. (2008). A similar behaviour is seen in this basin for *u*LSW, while SAIW shows a steadier rate throughout 1981–2006 of 0.62 ± 0.03 µmol kg^{-1} yr^{-1}, which is near twice the observed rate of *u*NADW and DSOW. This same recurring tendency of fast rates of increase for C_{ant} concentrations during 1991–1997 and later the slowdown during the OVIDE era, is observed for the rest of the transient tracers studied in the Irminger basin (Kieke et al., 2006).

Table 3. The C_{ant} storage rates ± standard error of the estimate for different NAO phases in the considered NASPG basins. The high NAO phase extends from 1989 to 1995 and the low NAO phase from 1996 to 2006. No cruise data for either 1989 or 1996 was available, therefore, data from the closest available years (1990/91 and 1997) was used for storage rate calculations for the high NAO phase (Fig. 3). In the Iceland basin the high NAO interval was further extended to 1998 for storage rate calculation purposes alone, given the shortage of data.

Basin	NAO Phase (time period)	C_{ant} Specific Inventory Rates (mol C m^{-2} yr^{-1})	C_{ant}Storage Rate (Gt C yr^{-1})
Irminger	High (1991–1997)	1.74 ± 0.18	0.013 ± 0.002
	Low(1997–2006)	0.4 ± 0.3	0.006 ± 0.002
Iceland	High (1991–1998)	1.88 ± 0.45	0.022 ± 0.005
	Low (1997–2006)	0.3 ± 0.2	0.0035 ± 0.003
ENA	(1981–2006)	0.72 ± 0.07	0.019 ± 0.002
NASPG (OVIDE box)	High NAO	1.18 ± 0.12	0.054 ± 0.006
	Low NAO	0.56 ± 0.08	0.026 ± 0.004

In the Iceland basin, the average C_{ant} concentrations of the SPMW increase monotonically over time by about 0.70 ± 0.08 µmol kg^{-1} yr^{-1} (Fig. 3b) during the whole period. The intermediate waters in this basin are represented by the upper and classical vintages of LSW. The average C_{ant} concentrations of *u*LSW show a steady increase from 1981 to 2006 (0.40 ± 0.06 µmol kg^{-1} yr^{-1}), while the concentrations in *c*LSW show two different temporal trends: on the one hand, there is a clear C_{ant} concentration increase from 1991 to 1998 (of $\sim 1.1 \pm 0.2$ µmol kg^{-1} yr^{-1}, i.e., about three times the mean rate for 1981–2006), but then the rise ceases and concentrations stabilise at a value of $\sim$25.6 µmol kg^{-1} from 1998 to 2006.

Concerning the deep layers of the Iceland basin (*u*NADW), the low AOU and [$Si(OH)_4$] values measured in the meridional cruises, conducted along 20° W (OACES-1993, CAOS-1998 and A16N-2003; Fig. 1a), reveal larger contributions of ISOW to the *u*NADW than from other cruises, which are mostly influenced by Antarctic Bottom Water (AABW). Such contributions account for the noticeable increase of C_{ant} concentrations ($\sim 0.42 \pm 0.09$ µmol kg^{-1} yr^{-1}) obtained in the deep layers of the Iceland basin. When the strong convection period relaxed afterwards (Lab Sea Group, 1998), this trend of C_{ant} increase also weakened, leaving a noisier pattern in C_{ant} increase tendencies. The effect of weaker convection on LSW propagates deep in the water column and it can be expected to affect NADW (Yashayaev et al., 2008).

The C_{ant} storage rate of the NACW layer (ENA basin) are the highest ones calculated in the NASPG (average 1.13 ± 0.14 µmol kg^{-1} yr^{-1}; Table 2c) and show a clear increase over the whole 1981–2006 time interval (Fig. 3c). The observed thermohaline trends (Fig. 2; Table 2c) for the NACW in the upper layers of the ENA basin are not as well defined as in the upper layers of the other two basins. The high convection events (AOU minima; Fig. 2; Table 2c), corresponding to 1990–1993 and 1998, are possibly linked with rapid responses in this region to the NAO shifts. Alternatively, it must be noticed that the cruises that sampled the south of the ENA basin (e.g. BD3 in 1989 or FOUREX in 1997) show the highest salinity values due to the important contributions of MW (Table 2c). There is a general increase in the MW layer of the average C_{ant} concentrations of 0.32 ± 0.02 µmol kg^{-1} yr^{-1}. The opposite (less MW influence and lower average salinity values) occurs for the A01E (1991) cruise that sampled the northern ENA basin. Most cruises in the ENA were conducted south of the basin (Fig. 1b) and, thus, the average values of θ, S and AOU (Table 2c) for the upper and intermediate waters (NACW and MW) are considerably higher than the climatological values, in general. In spite of having applied the sampling sparseness correction for C_{ant} estimates in the ENA basin (Eq. 2), it is very likely that some bias (high C_{ant} values) has remained, given that the south ENA basin has been sampled more often than the north.

The LSW layer in the ENA basin shows a quite constant rate of C_{ant} increase (0.34 ± 0.03 µmol kg^{-1} yr^{-1}) throughout the whole 1981–2006 time interval. The presence of LSW in the ENA basin is well traced by the low AOU and [$Si(OH)_4$] values. The LSW in the ENA basin fades progressively towards the Iberian Peninsula, where the BD3 shows the LSW θ and S maximum values compared to what is observed in the rest of the basin, i.e., a homogeneous distribution of such tracers (Table 2c). The low AOU signal in 1991 and 1993 stems from the fast and far-reaching spreading of LSW after the strong convection period that occurred during that time (Read and Gould, 1992; Sy et al., 1997).

The temporal trends of the average C_{ant} concentrations in the deep waters of the ENA basin (*u*NADW and *l*NADW) are very similar. As expected from their location in the water column, far from upper layer influences, their C_{ant} concentrations are the lowest ones found in the study area. Actually, no significant trends of C_{ant} increase are detected. However, the average concentrations of C_{ant} in these two

layers for the 1981–2006 period (Table 2c) are somewhat different: 9.6 ± 1.1 and $5.1 \pm 1.0\,\mu mol\,kg^{-1}$ for the *u*NADW and *l*NADW, respectively. The warm component of NADW (*u*NADW) is less influenced by AABW than the cold component (*l*NADW), as reflected by the low $[Si(OH)_4]$ values of the former compared with those of the latter. Also, the higher influence of LSW/ISOW in the *u*NADW is revealed by its imprint in the AOU and $[Si(OH)_4]$ values, which are lower than the observed in the *l*NADW layer.

4.2 C_{ant} storage rates in the NASPG between 1981 and 2006

In the Irminger basin, the obtained results are similar to those in Pérez et al. (2008), i.e., there is a large decadal variability in the C_{ant} storage rates. During the early 1990s, the rate of change in the total inventory of C_{ant} ($0.013 \pm 0.002\,Gt\,C\,yr^{-1}$) is almost twice the average for 1981–2006, whilst a remarkable drop to about half this value ($0.006 \pm 0.002\,Gt\,C\,yr^{-1}$) followed from 1997 onwards, mostly due to the lower contribution from the LSW, which is the most influential water mass in the Irminger Sea. The NAO shift from a positive to a negative phase in 1996 led to a reduction of the air-sea heat loss in the Labrador Sea. The consequential convection weakening accompanied by a strong stratification are the main reasons for the overall decline of the northern North Atlantic CO_2 sink.

The latter argumentation, linking the contribution of LSW and the variability of C_{ant} total inventories, is consistent with the temporal variability of layer thicknesses shown in Fig. 5a. It is indeed observed that the volumetric census of *c*LSW reaches a peak during the first half of the 1990s. Interestingly, the thickness of the *u*LSW is out of phase with respect to the *c*LSW thickness peaks (Fig. 5a). Also, the development of the *u*NADW appears to follow that of the *u*LSW, suggesting that the volumetric census of this deeper layer is modulated by the strength of the convective activity in the Labrador Sea and Irminger basin too, which ultimately determines the extent of *c*LSW formation.

During the early 90s, the strong convection processes in the Labrador and Irminger Sea (Yashayaev et al., 2008) favoured the transformation of some *u*LSW (upper 1000 m) and *u*NACW (below 1500 m) into *c*LSW. Such transformation and the increase of advected *c*LSW also support a downstream increase (from the Irminger towards the Iceland basin) of the mixing between *u*NACW and *c*LSW, thus, reducing the *u*NACW thickness. During low convection periods, the *c*LSW penetration reduces and the reduced mixing favours the thickening of *u*LSW and *u*NADW at the expense of *c*LSW, in both the Irminger and Iceland basins. The lower C_{ant} concentrations of the *u*NACW, compared to those in *c*LSW, lead to larger C_{ant} inventories when the thickness of LSW increases with respect to the *u*NACW one. The *u*LSW and *c*LSW have similar C_{ant} concentrations and, therefore,

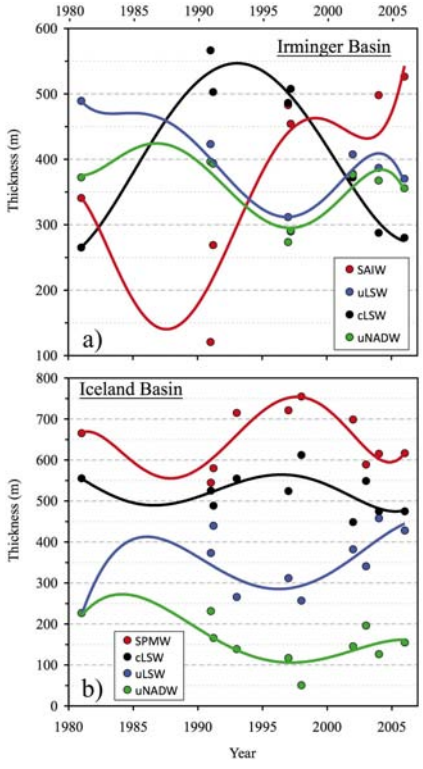

Fig. 5. Scatter plots with overlaid polynomial fits of different orders showing the temporal evolution of layer thicknesses in the Irminger (5a) and Iceland (5b) basins. The thicknesses were calculated applying Eq. (A4) given in Appendix A1. The Iceland basin shows a thicker, more developed *c*LSW layer than in the Irminger basin given the deeper bathymetry of the former and also because *c*LSW forms mainly in the Irminger, but develops further towards the Iceland basin. The propagation of Irminger formed waters into the Iceland basin is also the reason for the slight temporal delay observed for the *c*LSW peak in the Iceland basin (towards 1997) with respect to the Irminger basin (where it occurs around 1993).

affect the variability of C_{ant} inventories to a lesser extent through variations of their respective thicknesses.

Therefore, from the above, the differences in North Atlantic C_{ant} storage rates between high and low NAO phases are attributed to the changes in C_{ant} concentrations and also to the decrease in the LSW volumetric census during the low NAO phase of 1997–2006 (Fig. 4b) rather than on an actual decrease of the amount of C_{ant} stored in the various water masses in this basin (Steinfeldt et al., 2009). This can be stated since inventories were calculated considering the temporal variability of thickness (Eq. 6; Table 2b).

On the other hand, the undersampling in the ENA basin, together with the high spatial variability of the specific inventories, masks the temporal trends that might have contributed to the observed changes of C_{ant} specific inventories driven mainly by shifts in the NAO phase. At the moment, our results do not provide solid evidence for a link between the NAO phase and the trends of C_{ant} inventory rates in the

ENA. By considering the same high and low NAO periods as in the Iceland Basin and applying Eq. (2) to calculate the specific inventories of C_{ant}, we obtained almost identical specific storage rates for the high and low NAO periods in the ENA basin, namely: $0.019_5 \pm 0.002$ (R^2=0.98) and 0.019 ± 0.005 (R^2=0.87) Gt C yr^{-1}, respectively. This is why a single storage rate for the whole 1981–2006 time period was calculated for the ENA basin, i.e., 0.019 ± 0.001 Gt C yr^{-1} (Table 3).

Very few studies can be used as benchmarks for our C_{ant} storage rates estimates in Table 3. Álvarez et al. (2003) (A'03 hereinafter) or Mikaloff-Fletcher et al. (2006) provide some indirect calculations in which to compare. Those mentioned studies have used C_{ant} transport and inventory estimates to calculate C_{ant} uptake rates from the atmosphere in "closed-box" type models for large oceanic regions, such as the North Atlantic. A'03 computed a constant C_{ant} storage rate of 0.07 ± 0.03 Gt C yr^{-1} for a region that is similar to the OVIDE box (Fig. 4), but with the FOUREX cruise as the southern bound of the box instead. This estimate, rescaled to our OVIDE box (considering the areas in Fig. 4) would amount to 0.044 ± 0.020 Gt C yr^{-1}, which is between our estimates of 0.054 ± 0.006 Gt C yr^{-1} (Table 3) during high NAO scenarios and 0.026 ± 0.004 Gt C yr^{-1} during the low NAO ones. Alternatively, Mikaloff-Fletcher et al. (2006) calculated, for the region enclosed between 49° N and 76° N, a constant C_{ant} storage rate of 0.11 ± 0.01 Gt C yr^{-1}. Applying the same scaling as for the result in A'03 and omitting the Nordic Seas, which alone represent 0.018 Gt C yr^{-1} (Jutterström et al., 2008)[1] in terms of C_{ant} storage rate, the Mikaloff-Fletcher et al. (2006) estimate for the OVIDE box would map to 0.064 ± 0.002 Gt C yr^{-1}. It must be remembered that, unlike in the present study, the works from A'03 and Mikaloff-Fletcher et al. (2006) both used a constant MPD approximation to calculate their steady-state C_{ant} storage rates.

Additionally, an assessment was performed on the impact or relative contribution for considering the temporal variability of layer thickness (Sect. 3.2 and Appendix A1) together with C_{ant} changes on the obtained inventory trends from Table 3. When the thickness variability is not taken into account in calculations, then the differences between high-NAO and low-NAO C_{ant} storage rates in the NASPG reduce by about 40%: from 0.028 Gt C yr^{-1} (Table 3) to 0.017 Gt C yr^{-1}. This result is consistent with what was found by Steinfeldt et al. (2009). In their Fig. 9, they showed how the fluctuations of LSW volume particularly affects the C_{ant} column inventory.

Lherminier et al. (2007) states that the intensity of the transport associated with the MOC does not have important variations from high to low NAO phases (19.2 ± 0.9 and 16.9 ± 1.0 Sv, respectively) in our study area. Knowing of this behaviour, a quasi-stationary state for the water mass transports within the upper limb of the MOC in the OVIDE box can be roughly assumed. Therefore, by considering: (a) the horizontal C_{ant} transports calculated in either A'03 or Mikaloff-Fletcher et al. (2006) of 0.04 and 0.02 Gt C yr^{-1}, respectively, and (b) the C_{ant} inventories calculated in our work, then the C_{ant} uptake rates from the atmosphere in low NAO phase scenarios would actually be strongly reduced or even turn positive, meaning that anthropogenic CO_2 outgasing from the ocean could be witnessed in the North Atlantic. This result encourages even more collaborative studies in the future that will examine simultaneously C_{ant} storage, transports and air-sea CO_2 fluxes in this region. Such research efforts will be assets to better understand and accurately assess the behaviour of the North Atlantic as an anthropogenic CO_2 source or sink in the future.

5 Conclusions

There is a generalised increase in C_{ant} burdens in the upper layers of the NASPG that responds to the atmospheric xCO_2 increase over time. The C_{ant} increase observed in intermediate layers (particularly LSW) is the result of the deep convective activity in the Subpolar North Atlantic that occurred during the first half of the 90s.

In the Irminger basin, the C_{ant} storage rates are influenced by the changes in the phase of the NAO. During the early 1990s, the rate of change in C_{ant} specific inventories (0.013 ± 0.002 Gt yr^{-1}) almost doubled the average in 1981–2006, whilst a remarkable drop to almost half that rate (0.006 ± 0.002 Gt yr^{-1}) followed from 1997 onwards, mostly due to the smaller LSW contributions during the low phase of NAO. In the Iceland basin, the differences in C_{ant} specific inventory rates for high-low NAO phases are even larger than in the Irminger. The reason for this result is twofolded: on the one hand, a decrease in the LSW volumetric census during the low NAO phase (1997–2006) has been observed, on the other hand, there exists a slowdown in C_{ant} storage rates for the uLSW and cLSW that was observed on a yearly basis during that same time period. Concerning the ENA, the deep waters (NADW) in the Iberian basin showed negligible changes in their C_{ant} storage rates, while the uppermost layers (NACW) store the largest C_{ant} concentrations of the NASPG and they also increase their average C_{ant} concentrations faster than any other water mass considered, on a yearly basis (1.13 ± 0.14 µmol kg^{-1} yr^{-1}).

[1] In order to calculate the storage rate from the inventory estimate of 1.2 Gt C provided by Jutterström et al. (2008) for the Nordic Seas, the expression proposed in in Tanhua et al. (2007) was applied, namely: Inventory=3.0·ΔC_{ant}. Hence, *Storage rate*=$\Delta C_{ant}/\Delta t = I/(\Delta t \cdot 3.0)$. The ΔC_{ant} calculations in Tanhua et al. (2007) were done for the period 1981–2004 (Δt=23 years) using an eMLR technique, while the ones in Jutterström et al. (2008) referred to 2002. A correction factor of 1.037 was calculated from the corresponding C_{ant} saturation values in 2002 and 2004. Thus, the value of 0.018 Gt C×yr^{-1} for the storage rate of the Nordic Seas reported here was calculated as $[I/(\Delta t \cdot 3.0)] \cdot 1.037 = [1.2\,\text{Gt C}/(3.0 \cdot 23\,\text{yr})] \cdot 1.037$.

The overall results indicate that during the high NAO phase that occurred in the first half of the 1990s, the C_{ant} storage rates in the NASPG are ∼48% higher than during the low NAO phase that followed (Table 3). This remarkable tendency suggests that a net decrease in the strength of the North Atlantic sink of atmospheric CO_2 has occurred between 1996 and 2006.

The changes in C_{ant} storage rates obtained here are consistent with the results in Omar and Olsen (2006), Corbière et al. (2007) and Schuster and Watson (2007), who found analogous decreasing rates in the air-sea CO_2 exchanges from surface fCO_2 measurements in the North Atlantic that, overall, contributed to the decrease of C_{ant} storage rates in the NASPG. Such air-sea CO_2 exchange results can be legitimately compared to the ones obtained here for C_{ant} storage rates since, according to Pérez et al. (2008), the cycles and uptake of natural and anthropogenic CO_2 in the NASPG are linked. Consequently, the observed decrease in air-sea CO_2 exchange over the last decade (Omar and Olsen, 2006; Corbière et al., 2007; Schuster et al., 2007) has occurred simultaneously and is most probably linked to the weakening of C_{ant} storage in the NASPG, as shown here (Sect. 4.2; Table 3), that stems from NAO-driven changes of stratification and convection intensity.

Appendix A

A1 Calculation of layer thickness ($Th^{*}_{b,l,c}$) for the water masses in the Irminger and Iceland basins

To quantify the variability of water mass formation rates through layer thickness values in the NASPG (Fig. 1b), we used two different sets of thickness data, namely: *Th* calculated from cruise data for a given layer "*l*" under cruise "*c*" in the Irminger and Iceland basins (denoted as $Th^{obs}_{b,l,c}$, listed in Table 2) and the analogous *Th* calculated from WOA05 climatological data (denoted as $Th^{WOA05}_{b,l,c}$, also listed in Table 2). If we take the ratio of each $Th^{obs}_{b,l,c}$ and $Th^{WOA05}_{b,l,c}$ with respect to the depth of the water column ($\sum_{l=1}^{k} Th^{obs}_{b,l,c}$ and $\sum_{l=1}^{k} Th^{WOA05}_{b,l,c}$, respectively) and calculate the quotient ($F_{b,l,c}$; Eq (A1)) then this value compares the observed thickness of layer "*l*" under the track of cruise "*c*" to the climatological value.

$$F_{b,l,c} = \frac{\%Th^{obs}_{b,l,c}}{\%Th^{WOA05}_{b,l,c}} = \frac{Th^{obs}_{b,l,c} \Big/ \sum_{l=1}^{k} Th^{obs}_{b,l,c}}{Th^{WOA05}_{b,l,c} \Big/ \sum_{l=1}^{k} Th^{WOA05}_{b,l,c}} \quad \text{(A1)}$$

The assumption here is that $F_{b,l,c}$ is constant everywhere (i.e., for any cruise "*c*") in the Irminger and Iceland basins, and it varies only from layer to layer and cruise to cruise (Table 2a and b). The $F_{b,l,c}$ values used are given in Table 2. This assumption can be justified since the Irminger and Iceland basins are relatively small (compared with the ENA basin) and are subject to strong mixing processes that tend to homogenize layer thicknesses in the whole area of the basin after each winter convection event. This means that the spatial variability of layer thickness in these two basins is rather small, while the temporal variability is quite large and is largely determined by the strength of winter convection.

There are some operational caveats to the above assumption. It must be noticed that $F_{b,l,c}$ values are not always identical at every station on a given cruise, layer and basin: there is a high short-scale spatial variability linked with the variability of the mesoscale field (Rodgers et al., 2009). In addition, the WOA05 gridded fields have been largely smoothed and have less spatial resolution ($1^\circ \times 1^\circ$, i.e., each of WOA05's pixels may include more than one station from the same cruise) than the observations from the cruises. In spite of everything, there is a reasonably good linear correspondence between $\%Th^{obs}_{b,l,c}$ and $\%Th^{WOA05}_{b,l,c}$ terms in Eq. (A1) (slopes range between 0.88 and 1.11). Even though the procedure introduced here to calculate C_{ant} inventories has certain caveats associated to it, it is still a more solid approach than the one previously used (Holfort et al., 1998; Roson et al., 2003; Álvarez et al., 2003) that assumed constant MPDs for a whole basin, based on the classical TSS concept from Keeling and Bolin (1967). It is also similar to the observations in Perez et al. (2008) that showed a variable MPD in the subpolar gyre.

The $F_{b,l,c}$ factor can then be used to obtain from the average climatological thickness of layer "*l*" in basin "*b*" ($Th^{WOA05}_{b,l}$; this is the WOA05 value in the "Cruise-Year" column in Table 2) an estimate of $Th_{b,l,c}$ much more representative of basin "*b*" (either Irminger or Iceland). The expression for $Th_{b,l,c}$ in (A2) basically scales the $Th^{WOA05}_{b,l}$ value accordingly with how representative $Th^{obs}_{b,l,c}$ is of average basin conditions, i.e., $F_{b,l,c}$.

$$Th_{b,l,c} = Th^{WOA05}_{b,l} \cdot F_{b,l,c} \quad \text{(A2)}$$

There is a caveat when calculating "$Th_{b,l,c}$" from the expression in (A2). This formulation does not ensure that $\sum_{l=1}^{k} Th^{obs}_{b,l,c} = \sum_{l=1}^{k} Th^{WOA05}_{b,l,c}$ in all cruises. This is due to the fact that the bathymetries recorded during the cruises may not necessarily coincide with those in the $1^\circ \times 1^\circ$ ETOPO2 database that had to be used for the climatological WOA05 calculations. Therefore, another minor correction needs to be done in order to ensure that the sum in Eq. (1) will always be done over the same bottom depth and, therefore, over the same total volume of the basin, irrespectively of the considered cruise. The basin standardization factor "$f_{b,c}$" in (A3) provides an expression to correct this effect. This correction was applied to the Irminger or Iceland basins in all inventory calculations (either specific or total) where the volume of the

Table A1. List of coefficients obtained for Eq. (A6) using the expression given in (A7) for each layer in the ENA basin. The constant terms "k" are not input parameters in (A6) and not reported. The information between brackets in the header line gives the associated "$i-$th" property and the units of the "a_i" coefficients. The "n.s." acronym stands for "not significant". The variables with this acronym explained very little of the $C_{\text{ant}}^{\text{ENA},l,c}$ variability and worsened the overall MLR fit. They were, therefore, rejected according to a stepwise method of MLR solving.

			Eastern North Atlantic (ENA) Basin			
Layer	R^2	Adj. R^2	a_1 (AOU; kg µmol^{-1})	a_2 (θ; °C^{-1})	a_3 (S)	a_4 (xCO$_2$; ppm^{-1})
NACW	0.97	0.97	n.s.	n.s.	n.s.	0.47 ± 0.03
MW	0.96	0.95	-0.31 ± 0.05	n.s.	17 ± 2	0.18 ± 0.02
LSW	0.90	0.86	-0.38 ± 0.20	-7.1 ± 3.3	n.s.	0.19 ± 0.02
uNADW	0.71	0.59	n.s.	-61 ± 18	$(0.7 \pm 0.2) \times 10^3$	0.06 ± 0.03
lNADW	0.41	0.36	-0.54 ± 0.21	n.s.	n.s.	n.s.

basin was calculated as the "$Area \cdot \sum_{l=1}^{k} Th_{b,l,c}$". The values obtained for $f_{b,c}$ were typically close to 1, which reaffirms that this factor introduces only a minor correction, yet is necessary from a formal and operational point of view.

$$f_{b,c} = \frac{\sum_{l=1}^{k} Th_{b,l,c}}{\sum_{l=1}^{k} Th_{b,l}^{\text{WOA05}}} \tag{A3}$$

Thus, Eq. (A2) upgrades to (A4) as follows:

$$Th_{b,l,c}^{*} = Th_{b,l,c} \cdot \frac{1}{f_{b,c}} \tag{A4}$$

This last expression is the one that was used to calculate the $Th_{b,l,c}^{*}$ terms in Eq. (1) to estimate the inventories of C_{ant} for the Irminger and Iceland basins.

A2 Correction of C_{ant} concentrations for the ENA basin ($^{*}C_{\text{ant}}^{\text{ENA},l,c}$).

The calculation procedure and assumptions outlined in Sect. A cannot be applied in the ENA basin since the weaker convection in this region makes the temporal variability of layer thickness much smaller compared to the Irminger and Iceland basins. Also, due to its larger extension and the sparseness of measurements in our study, the factor $F_{b,l,c}$ in the ENA basin is always taken as 1, i.e., $Th_{\text{ENA},l,c} = Th_{\text{ENA},l}^{\text{WOA05}}$.

In the case of the ENA basin, the "$C_{\text{ant}}^{\text{ENA},l,c}$" terms were corrected to better represent the C_{ant} values in each considered layer of the basin (Fig. 1b) by adding to the previously calculated "$C_{\text{ant}}^{\text{ENA},l,c}$" a new term named as "$\Delta C_{\text{ant}}^{\text{ENA},l,c}$" (Eq. A5). This new term represents the deviation of "$C_{\text{ant}}^{\text{ENA},l,c}$" (calculated from cruise data) from basin averages at the time of the cruise.

$$^{*}C_{\text{ant}}^{\text{ENA},l,c} = C_{\text{ant}}^{\text{ENA},l,c} + \Delta C_{\text{ant}}^{\text{ENA},l,c} \tag{A5}$$

The (A5) expression was used to calculate the $^{*}C_{\text{ant}}^{\text{ENA},l,c}$ terms in Eq. (2). The "$\Delta C_{\text{ant}}^{\text{ENA},l,c}$" terms are computed using an extrapolation method based on covariations with WOA05 properties. These small "$\Delta C_{\text{ant}}^{\text{ENA},l,c}$" biases are expectable because, for each layer, a spatial gradient in C_{ant} exists in the ENA due to the different ventilation stages and rates of each water mass. As a matter of fact, the AOU in the ENA basin displays a positive southward gradient for all layers. Perez et al. (2008) found, for the Irminger basin, a clear relationship between AOU (a proxy for ventilation) and C_{ant} saturation for different water masses. The "$\Delta C_{\text{ant}}^{\text{ENA},l,c}$" terms were computed from cruise data and expressed as individual correction elements for each cruise and layer in the ENA basin as follows:

$$\Delta C_{\text{ant}}^{\text{ENA},l,c} = \sum_{i=1}^{3} a_i \left(X_i^{\text{WOA05},l,c} - X_i^{\text{ENA},l,c} \right) \tag{A6}$$

Where subscript "i" denotes "property", namely: 1=AOU; 2=θ; 3=S. The "X_i^c" and "X_i^{WOA05}" terms are the average magnitudes of the "ith" property from direct observations and from the WOA05 data at the same location of the considered cruise track, respectively (Table 2). The "a_i" factors are the regression coefficients, which are calculated in the ENA basin for each layer from an MLR fit (Eq. A7) of the C_{ant} averages ($C_{\text{ant}}^{\text{ENA},l,c}$) vs. the "$i$" properties using data from the eleven available cruises (Table 2c). The obtained "a_i" regression coefficients are listed in Table A1.

$$\text{MLR } C_{\text{ant}}^{\text{ENA},l,c} = \sum_{i=1}^{4} a_i X_i^{\text{ENA},l,c} + k \tag{A7}$$

All terms and scripts in Eq. (A7) have the same meaning as in (A6). Silicate was initially contemplated as a proxy for the influence of Antarctic waters, but no significant correlations were obtained and it was, therefore, discarded from the fit. The X_4 term is the $x\text{CO}_2^{\text{atm}}$ for the year of the corresponding cruise "c". The $x\text{CO}_2^{\text{atm}}$ time series records were obtained

from selected meteorological stations of the global cooperative air-sampling network managed and operated by the National Oceanic and Atmospheric Administration (NOAA; http://www.esrl.noaa.gov/gmd/ccgg/flask.html) Carbon Cycle Greenhouse Gas group. It must be noticed that the "a_4" term in Table A1 associated with the xCO_2^{atm} variable in (A7) is not used in (A6) since the $\Delta C_{ant}^{ENA,l,c}$ term only includes the effects of variables with spatial variation. Such xCO_2^{atm} terms are, however, mandatory when calculating the "a_i" coefficients (Eq. (A7); Table A1), since xCO_2^{atm} has a strong co-variation with C_{ant}. Having "a_4" included in (A7) removes "a_i" factors from the rest of the transient influences which certainly co-vary with $C_{ant}^{ENA,l,c}$. With the result that more robust MLR coefficients are obtained.

Appendix B

B1 Evaluation of C_{ant} inventory uncertainties

There are two major sources of uncertainties in the calculation of C_{ant} inventories (and, thus, storage rates) in our work: (a) The uncertainties associated with the C_{ant} estimation method; (b) The uncertainties associated with the calculation of layer thickness.

Table B1 given below includes the specific inventory rates of C_{ant} (mol C m^{-2} yr^{-1})$\pm$ the standard errors of the estimate calculated in three additional ways to the way it was finally done in our study and given in Table 3 (single linear regression):

1. Column "Perturbation $2\sigma C_{ant}$ method": The standard errors of the C_{ant} estimates obtained for each cruise and layer (given in Table 2 a, b, c) were randomly propagated 100 times. Afterwards, the average $\pm$ standard deviation of all 100 slopes was calculated. This is the value shown in column 4 of the Table B1. The uncertainty in C_{ant} estimation when applying the φ C_T° method is $\pm$ 5.2 µmol kg^{-1}, as mentioned in Sect. 3.1.

2. Column "Perturbation 2σ *Th* factor": The standard errors of the $F_{b,l,c}$ estimates obtained for each cruise and layer (given in Table 2a and b) in the Irminger and Iceland basins were randomly propagated 100 times. In the case of the ENA basin, the *Th* calculated from WOA05 data is applied ($F_{ENA,l,c}$ =1), so a constant error of 5% is assumed. Afterwards, the average $\pm$ standard deviation of all 100 slopes was calculated. This is the value shown in column 5 of the Table B1.

3. Column "Perturbation C_{ant} and *Th*": Both sources of error in the previous two columns are combined and then randomly propagated 100 times to get, again, the average $\pm$ standard deviation of all 100 slopes. This is the value shown in column 6 of the Table B1.

In the case of the ENA basin, the standard error in column 6 of Table B1 ($\pm$ 0.07) is larger than the one given in column 3 ($\pm$ 0.03), obtained from simple linear regression of C_{ant} inventory vs. time. Thus, Table 3 gives the largest standard error of these two values for the C_{ant} inventory rate in the ENA: 0.72 ± 0.07 mol C m^{-2} yr^{-1} (Table 3). The opposite occurred in the cases of the Irminger and Iceland basins (standard errors in column 3 are larger than those in column 6). Again, the largest standard error is reported in Table 3 so that the upper limits of our uncertainty sources are always provided.

B2 Comparison of C_{ant} inventory rates from two independent calculation methodologies: The φC_T° method and the TrOCA approach

The choice of the C_{ant} estimation method to be applied was to a large degree subject to the available variables measured during the cruises in the selected dataset (Table 1; Sect. 2). The TTD (Waugh et al., 2006) and ΔC* (Gruber et al., 1996) methods both need CFC data to make their estimates. Since most cruises in the dataset did not include these measurements, these two candidates could not be used in our study to estimate C_{ant}. On the other hand, the eMLR method (Tanhua et al., 2006) is based on repeated sections over time, which we did not have in our case except for the meridional cruises TYRO (1990), OACES (1993), CHAOS (1998) and A16N (2003). Unfortunately, these cruises only covered a small area of the Iceland and ENA basins. The C_{IPSL}° method from Lo Monaco et al. (2005) was proven to yield consistently higher estimates in the Atlantic than the ΔC*, TTD, TrOCA (Touratier et al., 2007) and φC_T° methods (Vázquez-Rodríguez et al., 2009). Hence, the only methodologies that could be successfully applied to our entire database are the φC_T° and TrOCA approaches.

Since the TrOCA method is very straightforward to apply, we estimated C_{ant} concentrations with it, performed the same calculations described in Sect. 3 and compared them with the results obtained from the φC_T° method (Table B2). The C_{ant} concentrations estimated with TrOCA were about 20% higher than those from the φC_T° method, as expected (Vázquez-Rodríguez et al., 2009; Yool et al., 2010). However, when comparing the trends in the C_{ant} storage rates, no statistical significant difference was found in most cases between the two sets of slopes (Table B2). This means that the choice of C_{ant} methodology does not have a significant influence on the results presented and discussed in this study, obtained with the φC_T° method.

Table B1. Standard errors of C_{ant} inventory estimates calculated considering the main sources of uncertainty involved, i.e., the uncertainty of C_{ant} concentration values and the uncertainty in layer thickness estimation (Appendix A1).
Specific Inventory Rates (mol C m^{-2} yr^{-1}): Slopes ± Std. errs.

Basin	NAO Phase	Linear regression (as in Table 3)	Pertubation ($2\sigma C_{ant}$ method)	Pertubation (2σ *Th* factor)	Pertubation (C_{ant} & *Th*)
Irminger	High (1991–1997)	1.74 ± 0.24	1.74 ± 0.15	1.73 ± 0.10	1.72 ± 0.19
	Low (1997–2006)	0.4 ± 0.3	0.43 ± 0.11	0.43 ± 0.05	0.43 ± 0.12
Iceland	High (1991–1998)	1.88 ± 0.45	1.85 ± 0.19	1.85 ± 0.16	1.85 ± 0.26
	Low (1997–2006)	0.3 ± 0.2	0.34 ± 0.12	0.34 ± 0.11	0.34 ± 0.17
ENA	(1981–2006)	0.72 ± 0.03	0.76 ± 0.05	0.76 ± 0.06	0.76 ± 0.07

Table B2. Comparison of results from two independent C_{ant} estimation methods. Overall, there is no statistically significant difference between the results derived from the TrOCA or the φC_T° methods.
Specific Inventory Rates (mol C m^{-2} yr^{-1})

Basin	NAO Phase (time period)	C_{ant} $\varphi C_T{}^\circ$	C_{ant} TrOCA
Irminger	High (1991–1997)	1.74 ± 0.24	1.88 ± 0.51
	Low (1997–2006)	0.40 ± 0.3	0.43 ± 0.31
Iceland	High (1991–1998)	1.88 ± 0.45	1.91 ± 0.76
	Low (1997–2006)	0.30 ± 0.2	0.55 ± 0.42
ENA	(1981–2006)	0.72 ± 0.03	0.76 ± 0.11

Acknowledgements. This work was developed and funded by the OVIDE research project from the French research institutions IFREMER and CNRS/INSU, by the European Commission within the 6th Framework Programme (EU FP6 CARBOOCEAN Integrated Project, Contract no. 511176), and by the Spanish research project M4AO (Modelo Multiparamétrico de mistura das masas de agua oceánicas PGIDIT07PXIB402153PR). We would like to extend our gratitude to the team who contributed in putting together the CARINA database and to the chief scientists, scientists and the crew who participated and put their efforts in the oceanographic cruises utilized in this study, particularly to those responsible for the carbon, CFC, and nutrient measurements. Marcos Vázquez-Rodríguez is funded by Consejo Superior de Investigaciones Científicas (CSIC) I3P predoctoral grant program REF.: I3P-BPD2005.

Edited by: J.-P. Gattuso

References

Álvarez, M., Rios, A. F., Perez, F. F., Bryden, H. L., and Roson, G.: Transports and budgets of total inorganic carbon in the subpolar and temperate North Atlantic, Global Biogeochem. Cy., 17(1), 1002, doi:10.1029/2002GB001881, 2003.

Azetsu-Scott, K., Jones, E. P., Yashayaev, I., and Gershey, R. M.: Time series study of CFC concentrations in the Labrador Sea during deep and shallow convection regimes (1991–2000), J. Geophys. Res., 108(C11), 3354, doi:10.1029/2002JC001317, 2003.

Böning C. W., Scheinert, M., Dengg, J., Biastoch, A., and Funk, A.: Decadal variability of subpolar gyre transport and its reverberation in the North Atlantic overturning, Geophys. Res. Lett., 33, L21S01, doi:10.1029/2006GL026906, 2006.

Bradshaw, A., Brewer, P., Shafer, D., and Williams, R.: Measurements of total carbon dioxide and alkalinity by potentiometric titration in the geosecs program, Earth Planet. Sci. Lett, 55, 99–115, 1981.

Broecker, W. S., Takahashi, T., Simpson, H. J., and Peng, T. H.: Fate of fosil fuel carbon dioxide and the global carbon budget, Science, 206, 409–418, 1979.

Bryden, H. L., Longworth, H. R., and Cunningham, S. A.: Slowing of the Atlantic meridional overturning circulation at 25° N, Nature, 438, 655–657, 2005.

Clayton, T. D. and Byrne, R. H.: Calibration of m-cresol purple on the total hydrogen ion concentration scale and its application to CO_2-system characteristics in seawater, Deep Sea Res. Pt. I, 40, 2115–2129, 1993.

Corbière, A., Metzl, N., Reverdin, G., Brunet, C., and Takahashi, T.: Interannual and decadal variability of the oceanic carbon sink in the North Atlantic subpolar gyre, Tellus, 59, 1–11, doi:10.1111/j.1600-0889.2006.00232, 2007.

Curry, R., McCartney, M. S., and Joyce, T. M.: Oceanic transport of subpolar climate signals to mid-depth tropical waters, Nature, 391, 575–577, 1998.

Dickson, A. G.: The measurement of sea water pH, Mar. Chem., 44, 131–142, 1993a.

Dickson, A. G.: pH buffers for sea water media based on the total hydrogen ion concentration scale, Deep-Sea Res., 40, 107–118, 1993b.

Dickson, A.G. and Millero, F.J.: A comparison of the equilibrium constants for the dissociation of carbonic acid in seawater media, Deep Sea Res. Pt. I, 34, 1733–1743, 1987.

Dickson, R. R., Lazier, J. R. N., Meincke, J., Rhines, P. B., and Swift, J. H.: Long-term coordinated changes in the convective activity of the North Atlantic, Prog. Oceanogr., 38, 241–295, 1996.

Dickson, R. R., Yashayaev, I., Meincke, J., Turrell, B., Dye, S., and Holfort, J.: Rapid freshening of the deep North Atlantic Ocean over the pastfour decades, Nature, 416, 832–837, 2002.

DOE, Handbook of the Methods for the Analysis of the Various Parameters of the Carbon Dioxide System in Sea Water, Version 2, ORNL/CDIAC-74, edited by: Dickson, A. G. and Goyet, C., 1994.

Drijfhout, S. S. and Hazeleger, W.: Changes in MOC and gyre-induced Atlantic Ocean heat transport, Geophys. Res. Lett., 33, L07707, doi:10.1029/2006GL025807, 2006.

Friis, K., Koertzinger, A., Patsch, J., and Wallace, D. W. R.: On the temporal increase of anthropogenic CO_2 in the subpolar North Atlantic, Deep Sea Res. Pt. I, 52, 681–698, 2005.

Gruber, N., Sarmiento, J. L., and Stocker, T. F.: An improved method for detecting anthropogenic CO_2 in the oceans, Global Biogeochem. Cy., 10, 809–837, 1996.

Häkkinen, S. and Rhines, P. B.: Decline of the subpolar North Atlantic circulation during the 1990s, Science, 204, 555–559, 2004.

Holfort, J., Johnson, K. M., Schneider, B., Siedler, G., and Wallace, D. W. R.: Meridional transport of dissolved inorganic carbon in the South Atlantic Ocean GBC, 12(3), 479-499, 1998.

IPCC: Summary for Policymakers, in: Climate Change 2007: Impacts, Adaptation and Vulnerability. Contribution of Working Group II to the Fourth Assessment Report of the Intergovernmental Panel on Climate Change, Cambridge University Press, Cambridge, UK, 7–22, http://ipcc-wg1.ucar.edu/wg1/wg1-report.html, 2007.

Johnson, G. C. and Gruber, N.: Decadal water mass variations along 20° W in the northeastern Atlantic Ocean, Prog. Oceanogr., 73, doi:10.1016/j.pocean.2006.03.022, 2007.

Johnson, K. M., Wills, K. D., Butler, D. B., Johnson, W. K., and Wong C. S.: Coulometric total carbon dioxide analysis for marine studies: Maximizing the performance of an automated continuous gas extraction system and coulometric detector, Mar. Chem., 44, 167–189, 1993.

Jutterström, S., Jeansson, E., Anderson, L. G., Bellerby, R., Jones, E. P, Smethie, W. M., and Swift, J. F.: Evaluation of anthropogenic carbon in the Nordic Seas using observed relationships of N, P and C versus CFCs, Prog. Oceanogr. 78, 78–84. 2008.

Keeling, C. D. and Bolin, B.: The simultaneous use of chemical tracers in oceanic studies, Tellus, 19, 566–581, 1967.

Kieke, D., Rhein, M., Stramma, L., Smethie, W. M., LeBel, D. A., and Zenk, W.: Changes in the CFC inventories and formation rates of Upper Labrador Sea Water, 1997–2001, J. Phys. Oceanogr., 36, 64–86, 2006.

Kieke, D., Rhein, M., Stramma, L., Smethie, W. M., Bullister, J. L., and LeBel, D. A.: Changes in the pool of Labrador Sea Water in the subpolar North Atlantic, Geophys. Res. Lett., 34, L06605, doi:10.1029/2006GL028959, 2007.

Latif, M., Böning, C. W., Willebrand, J., Biastoch, A., Dengg, J., Keenlyside, N., and Schweckendiek, U.: Is the thermohaline circulation changing?, J. Climate, 19, 4631–4637, 2006.

Lazier, J., Hendry, R., Clarke, R. A., Yashayaev, I., and Rhines, P.: Convection and restratification in the Labrador Sea, 1990–2000, Deep-Sea Res., 49, 1819–1835, 2002.

Le Quéré, C, Raupach, M. R., Canadell, J. G., Marland, G., et al.: Trends in the sources and sinks of carbon dioxide, Nat. Geosci., 2, 831–836, doi:10.1038/ngeo689, 2009.

Lee, K., Choi, S.-D., Park, G.-H., Wanninkhof, R., Peng, T.-H. R., Key, M., Sabine, C. L., Feely, R. A., Bullister, J. L., Millero, F. J., and Kozyr, A.: An updated anthropogenic CO_2 inventory in the Atlantic Ocean, Global Biogeochem. Cy., 17(4), 1116, doi:10.1029/2003GB002067, 2003.

Lo Monaco, C., Metzl, N., Poisson, A., Brunet, C., and Schauer, B.: Anthropogenic CO_2 in the SO: Distribution and inventory at the Indian-Atlantic boundary (World Ocean Circulation Experiment line I6), J. Geophys. Res., 110, C06010, doi:10.1029/2004JC002643, 2005.

Lherminier, P., Mercier, H., Gourcuff, C., Alvarez, M., Bacon, S., and Kermabon, C.: Transports across the 2002 Greenland-Portugal Ovide section and comparison with 1997, J. Geophys. Res., 112, C07003, doi:10.1029/2006JC003716, 2007.

Marshall, J., Dobson, F., Mooer, K., et al.: The Labrador Sea Deep Convection Experiment, B. Am. Meteorol. Soc., 79(10), 2033–2058, 1998.

Mikaloff-Fletcher, S. E., Gruber, N., Jacobson, A. R., Doney, S. C., Dutkiewicz, S., Gerber, M., Follows, M., Joos, F., Lindsay, K., Menemenlis, D., Mouchet, A., Müller, S. A., and Sarmiento, J. L.: Inverse estimates of anthropogenic CO_2 uptake, transport, and storage by the ocean, Global Biogeochem. Cy., 20, GB2002, doi:10.1029/2005GB002530, 2006.

Millero, F. J.: The marine inorganic carbon cycle, Chem. Rev., 107, 308–341, 2007.

Millero, F. J., Zhang, J. Z., Lee, K., and Campbell, D. M.: Titration alkalinity of seawater, Mar. Chem., 44, 153–156, 1993.

Mintrop, L., Perez, F. F., Gonzalez-Davila, M., Santana-Casiano, M. J., and Kortzinger, A.: Alkalinity determination by potentiometry: Intercalibration using three different methods, Ciencias Marinas 26(1), 23–37, 2002.

Omar, A. M. and Olsen, A.: Reconstructing the time history of the airsea CO_2 disequilibrium and its rate of change in the eastern subpolar North Atlantic, 1972–1989, Geophys. Res. Lett., 33, L04602, doi:10.1029/2005GL025425, 2006.

Ono, T, Watanabe, S., Okuda, K., and Fukasawa, M.: Distribution of total carbonate and related properties in the North Pacific along 30° N, J. Geophys. Res., 103, 308, 73–83, 1998.

Pérez, F. F. and Fraga, F.: A precise and rapid analytical procedure for alkalinity determination, Mar. Chem., 21, 169–182, 1987.

Pérez F. F., Álvarez , M., and Ríos, A. F.: Improvements on the back-calculation technique for estimating anthropogenic CO_2, Deep-Sea Res. Pt. I, 49/5, 859–875, 2002.

Pérez, F. F., Vázquez-Rodríguez, M., Louarn, E., Padn, X. A., Mercier, H., and Ríos, A. F.: Temporal variability of the anthropogenic CO_2 storage in the Irminger Sea, Biogeosciences, 5, 1669–1679, doi:10.5194/bg-5-1669-2008, 2008.

Pickart, R. S., Straneo, F., and Moore, G. W. K.: Is Labrador Sea Water formed in the Irminger Basin? Deep-Sea Res. Pt. I, 50, 23–52, 2003.

Pierrot, D., Brown, P., van Heuven, S., Tanhua, T., Schuster, U., Wanninkhof, R., and Key, R.: CARINA TCO_2 Data in the Atlantic Ocean. Earth System Science Data (ESSD), Earth Syst. Sci. Data Discuss., 3, 1–26, 2010, http://www.earth-syst-sci-data-discuss.net/3/1/2010/.

Read, J. F. and Gould, W. J.: Cooling and freshening of the subpolar

North Atlantic Ocean since the 1960s, Nature, 360, 55–57, 1992.
Rodgers, K. B., Key, R. M., Gnanadesikan, A., Sarmiento, J. L., Aumont, O., Bopp, L., Doney, S. C., Dunne, J. P., Glover, D. M., Ishida, A., Ishii, M., Jacobson, A. R., Lo Monaco, C., Maier-Reimer, E., Mercier, H., Metzl, N., Perez, F. F., Rios, A. F., Wanninkhof, R., Wetzel, P., Winn, C. D., and Yamanaka, Y.: Altimetry helps to explain patchy changes in hydrographic carbon measurements, J. Geophys. Res,-Oceans, 114, C09013, doi:10.1029/2008JC005183, 2009.
Roson, G., Rios, A. F., Perez, F. F., Lavin, A., and Bryden, H. L.: Carbon distribution, fluxes, and budgets in the subtropical North Atlantic Ocean (24.5° N), J. Geophys. Res., 108(C5), 3144, doi:10.1029/1999JC000047, 2003.
Sabine, C. L., Feely, R. A., Gruber, N., Key, R. M., Lee, K., Bullister, J. L., Wanninkhof, R., Wong, C. S., Wallace, D. W. R., Tilbrook, B., Millero, F. J., Peng T.-H., Kozyr, A., Ono, T., and Ríos, A. F.: The oceanic sink for anthropogenic CO_2, Science, 305, 367–371, 2004.
Sarafanov, A., Falina, A., Sokov, A., and Demidov, A.: Intense warming and salinification of intermediate waters of southern origin in the eastern subpolar North Atlantic in the 1990s to mid-2000s, J. Geophys. Res., 113, C12022, doi:10.1029/2008JC004975, 2008.
Sarafanov, A., Sokov, A., Demidov, A., and Falina, A.: Warming and salinification of intermediate and deep waters in the Irminger Sea and Iceland Basin in 1997–2006, Geophys. Res. Lett., 34, L23609, doi:10.1029/2007GL031074, 2007.
Sarmiento, J. L. and Le Quéré, C.: Oceanic carbon dioxide uptake in a model of century-scale global warming, Science, 274, 1346–1350, 1996.
Schuster, U. and Watson, A. J.: A variable and decreasing sink for atmospheric CO_2 in the North Atlantic, J. Geophys. Res., 112,C11006, doi:10.1029/2006JC003941, 2007.
Steinfeldt, R., Rhein, M., Bullister, J. L., and Tanhua, T.: Inventory changes in anthropogenic carbon from 1997–2003 in the Atlantic Ocean between 20° S and 65° N, Global Biogeochem. Cy., 23, GB3010, doi:10.1029/2008GB003311, 2009.
Swingedouw, D., Bopp, L., Matras, A., and Braconnot, P.: Effect of land-ice melting and associated changes in the AMOC result in little overall impact on oceanic CO_2 uptake, Geophys. Res. Lett., 34, L23706, doi:10.1029/2007GL031990, 2007.
Sy, A., Rhein, M., Lazier, J. R. N., Koltermann, K. P., et al.: Surprisingly rapid spreading of newly formed intermediate waters across the North Atlantic Ocean, Nature, 386, 675–679, 1997.
Tanhua, T., Biastoch, A., Körtzinger, A., Lüger, H., Böning, C., and Wallace, D. W. R.: Changes of anthropogenic CO_2 and CFCs in the North Atlantic between 1981 and 2004, Global Biogeochem. Cy., 20, GB4017, doi:10.1029/2006GB002695, 2006.
Tanhua, T., Körtzinger, A., Friis, K., Waugh, D. W., and Wallace, D. W. R.: An estimate of anthropogenic CO_2 inventory from decadal changes in oceanic carbon content, PNAS, 104(9), 3037–3042, 2007.
Tanhua, T., Olsson, K. A., and Jeansson, E.: Tracer evidence of the origin and variability of Denmark Strait OverflowWater, in: Arctic-Subarctic Ocean Fluxes: Defining the role of the Nordic Seas in Climate, edited by: Dickson, R. R., Meincke, J., and Rhines, P., pp. 475–503, Springer Verlag, 2008.
Tanhua, T. and Wallace, D. W. R.: Consistency of TTO-NAS inorganic carbon data with modern measurements, Geophys. Res. Lett., 32, L14618, doi:10.1029/2005GL023248, 2005.
Thierry, V., de Boisséson, E., and Mercier, H., Interannual variability of the Subpolar Mode Water properties over the Reykjanes Ridge during 1990–2006, J. Geophys. Res., 113, C04016, doi:10.1029/2007JC004443, 2008.
Touratier, F., Azouzi, L., and Goyet, C.: CFC-11, Δ14C and 3H tracers as a means to assess anthropogenic CO_2 concentrations in the ocean, Tellus, 59B, 318–325, doi:10.1111/j.1600-0889.2006.00247.x, 2007.
Vázquez-Rodríguez, M., Padin, X. A., Ríos, A. F., Bellerby, R. G. J., and Pérez, F. F.: An upgraded carbon-based method to estimate the anthropogenic fraction of dissolved CO_2 in the Atlantic Ocean, Biogeosciences Discuss., 6, 4527–4571, doi:10.5194/bgd-6-4527-2009, 2009.
Vázquez-Rodríguez, M., Touratier, F., Lo Monaco, C., Waugh, D. W., Padin, X. A., Bellerby, R. G. J., Goyet, C., Metzl, N., Ríos, A. F., and Pérez, F. F.: Anthropogenic carbon distributions in the Atlantic Ocean: data-based estimates from the Arctic to the Antarctic, Biogeosciences, 6, 439–451, doi:10.5194/bg-6-439-2009, 2009.
Velo, A., Perez, F. F., Brown, P., Tanhua, T., Schuster, U., and Key, R. M.: CARINA alkalinity data in the Atlantic Ocean, Earth Syst. Sci. Data, 1, 45–61, 2009a, http://www.earth-syst-sci-data.net/1/45/2009/.
Velo, A., Pérez, F. F., Lin, X., Key, R. M., Tanhua, T., de la Paz, M., van Heuven, S., Jutterström, S., and Ríos, A. F.: CARINA data synthesis project: pH data scale unification and cruise adjustments, Earth Syst. Sci. Data Discuss., 2, 421–475, 2009b, http://www.earth-syst-sci-data-discuss.net/2/421/2009/.
Waugh, D. W., Hall, T. M., McNeil, B. I., Key, R., and Matear, R. J.: Anthropogenic CO_2 in the oceans estimated using transit time distributions, Tellus B, 58B, 376–389, doi:10.1111/j.1600-0889.2006.00222.x, 2006.
Yashayaev, I., Holliday, N. P., Bersch, M., and van Aken, H. M.: The history of the Labrador Sea Water: Production, Spreading, Transformation and Loss. In "Arctic-Subarctic Ocean Fluxes: defining the role of the Northern Seas in climate", edited by: Robert, R., Dickson, J., and Meincke, P., Rhines. Springer, P.O. Box 17, 3300 AA Dordrecht, The Netherlands, pp. 569–612, 2008.
Yashayaev, I., van Aken, H. M., Holliday, N. P., and Bersch, M.: Transformation of the Labrador Sea Water in the subpolar North Atlantic, Geophys. Res. Lett., 34 , L22605, doi:10.1029/2007GL031812, 2007.
Yool, A., Oschlies, A., Nurser, A. J. G., and Gruber, N.: A model-based assessment of the TrOCA approach for estimating anthropogenic carbon in the ocean, Biogeosciences, 7, 723–751, doi:10.5194/bg-7-723-2010, 2010.